

THE CONVECTIVE HEAT TRANSFER BEHAVIOR
OF A HEATED CYLINDER LOCATED NEAR A
PLANE SURFACE

Charles Henry Gnerlich

NAVAL POSTGRADUATE SCHOOL

Monterey, California



THESIS

The Convective Heat Transfer Behavior
Of A
Heated Cylinder Located Near A Plane Surface

by

Charles Henry Gnerlich

June 1975

Thesis Advisor:

Thomas E. Cooper

Approved for public release; distribution unlimited.

T 167473



UNCLASSIFIED

SECURITY CLASSIFICATION OF THIS PAGE (When Data Entered)

REPORT DOCUMENTATION PAGE		READ INSTRUCTIONS BEFORE COMPLETING FORM
1. REPORT NUMBER	2. GOVT ACCESSION NO.	3. RECIPIENT'S CATALOG NUMBER
4. TITLE (and Subtitle) The Convective Heat Transfer Behavior of a Heated Cylinder Located Near a Plane Surface		5. TYPE OF REPORT & PERIOD COVERED Master's Thesis; June 1975
7. AUTHOR(s) Charles Henry Gnerlich		6. PERFORMING ORG. REPORT NUMBER
9. PERFORMING ORGANIZATION NAME AND ADDRESS Naval Postgraduate School Monterey, CA 93940		8. CONTRACT OR GRANT NUMBER(s)
11. CONTROLLING OFFICE NAME AND ADDRESS Naval Postgraduate School Monterey, CA 93940		10. PROGRAM ELEMENT, PROJECT, TASK AREA & WORK UNIT NUMBERS
14. MONITORING AGENCY NAME & ADDRESS (if different from Controlling Office) Naval Postgraduate School Monterey, CA 93940		12. REPORT DATE June 1975
		13. NUMBER OF PAGES 73
		15. SECURITY CLASS. (of this report) UNCLASSIFIED
		15a. DECLASSIFICATION/DOWNGRADING SCHEDULE
16. DISTRIBUTION STATEMENT (of this Report) Approved for public release; distribution unlimited.		
17. DISTRIBUTION STATEMENT (of the abstract entered in Block 20, if different from Report)		
18. SUPPLEMENTARY NOTES		
19. KEY WORDS (Continue on reverse side if necessary and identify by block number)		
20. ABSTRACT (Continue on reverse side if necessary and identify by block number) An experimental apparatus which will allow the study of the influence of ground effects on a heated cylinder placed in a crossflow of air was designed and constructed. The effects of a wall on the heat transfer characteristics of a heated cylinder were investigated at a Reynolds number of 153,000 for cylinder to wall spacings ranging from $dr/ = 0.0$		

UNCLASSIFIED

SECURITY CLASSIFICATION OF THIS PAGE (When Data Entered)



20. Abstract (continued)

to $d/r = 5.33$ (maximum), where d = gap width, and r = cylinder radius. Pressure coefficients were obtained at five degree intervals around the cylinder for each experiment.

Experimental results obtained for $d/r = 0.0$ agreed well with previously reported investigations of a cylinder attached to a wall. Results obtained for $d/r = 5.33$ agreed well with previous work done with free cylinders. Experiments conducted at intermediate values of d/r resulted in minimum and maximum average Nusselt numbers, suggesting that gap spacing may exert a strong influence on the behavior of the flow field.

The Convective Heat Transfer Behavior
Of A
Heated Cylinder Located Near A Plane Surface

by

Charles Henry Gnerlich
Lieutenant, United States Navy
B.M.E., University of Louisville, 1966

Submitted in partial fulfillment of the
requirements for the degree of

MASTER OF SCIENCE IN MECHANICAL ENGINEERING

from the

NAVAL POSTGRADUATE SCHOOL

June 1975

Thesis
G 521
C. 2

ABSTRACT

An experimental apparatus which will allow the study of the influence of ground effects on a heated cylinder placed in a crossflow of air was designed and constructed.

The effects of a wall on the heat transfer characteristics of a heated cylinder were investigated at a Reynolds number of 153,000 for cylinder to wall spacings ranging from $d/r = 0.0$ to $d/r = 5.33$ (maximum), where d = gap width, and r = cylinder radius. Pressure coefficients were obtained at five degree intervals around the cylinder for each experiment.

Experimental results obtained for $d/r = 0.0$ agreed well with previously reported investigations of a cylinder attached to a wall. Results obtained for $d/r = 5.33$ agreed well with previous work done with free cylinders. Experiments conducted at intermediate values of d/r resulted in minimum and maximum average Nusselt numbers, suggesting that gap spacing may exert a strong influence on the behavior of the flow field.

TABLE OF CONTENTS

I.	INTRODUCTION -----	9
II.	BACKGROUND -----	13
III.	EXPERIMENTAL APPARATUS -----	15
	A. WIND TUNNEL -----	15
	B. HEAT TRANSFER EXPERIMENT -----	17
	C. PRESSURE COEFFICIENT EXPERIMENT -----	20
IV.	EXPERIMENTAL PROCEDURE -----	23
	A. HEAT TRANSFER EXPERIMENT -----	24
	B. PRESSURE COEFFICIENT EXPERIMENT -----	26
V.	RESULTS -----	28
VI.	CONCLUSIONS AND RECOMMENDATIONS -----	48
	APPENDIX A - HEAT TRANSFER AND PRESSURE DATA REDUCTION -	49
	APPENDIX B - UNCERTAINTY ANALYSIS -----	53
	APPENDIX C - HOT WIRE ANEMOMETER CALIBRATION -----	59
	APPENDIX D - WIND TUNNEL VELOCITY PROFILE AND TURBULENCE INTENSITY -----	64
	LIST OF REFERENCES -----	72
	INITIAL DISTRIBUTION LIST -----	73



LIST OF ILLUSTRATIONS

1.	Schematic diagram showing determination of d/r ----	11
2.	Schematic diagram of the wind tunnel -----	16
3.	Photograph of the Tensheet cylinder -----	18
4.	Photograph of the plate and cylinder assembly -----	21
5.	Photograph of the cylinder used to collect pressure data -----	22
6.	Comparison of the heat transfer results for $d/r = 0.0$ with the results of McComas at $Re = 153,000$ -----	29
7.	Comparison of the heat transfer results for $d/r = 5.33$ and $Re_{corr} = 161,000$ with the results of field at $Re = 148,000$ and with the theory of Schuh -----	31
8.	Shift of the Laminar separation points and the stagnation point with increasing d/r -----	33
9.	Comparison of the local Nusselt number at $d/r = 0.0$ with the local Nusselt number at $d/r = 0.25$ -----	35
10.	Comparison of the pressure coefficient at $d/r = 0.0$ with the pressure coefficient at $d/r = 0.25$ -----	36
11	(a) Average Nusselt number versus d/r -----	37
	(b) Maximum Nusselt numbers on the front and back of the cylinder versus d/r -----	37
12.	Voltage required to maintain a predetermined temperature at the positions of 150 and 165 degrees versus d/r -----	39
13.	Polar plot of Nusselt number and pressure coefficient versus angle for $d/r = 0.0$ -----	41
14.	Polar plot of Nusselt number and pressure coefficient versus angle for $d/r = 0.25$ -----	42
15.	Polar plot of Nusselt number and pressure coefficient versus angle for $d/r = 0.5$ -----	43

16.	Polar plot of Nusselt number and pressure coefficient versus angle for $d/r = 1.0$ -----	44
17.	Polar plot of Nusselt number and pressure coefficient versus angle for $d/r = 2.0$ -----	45
18.	Polar plot of Nusselt number and pressure coefficient versus angle for $d/r = 4.0$ -----	46
19.	Polar plot of Nusselt number and pressure coefficient versus angle for $d/r = 5.33$ -----	47
20.	Voltage squared versus the square root of velocity for hot wire anemometer calibration -----	63
21.	Isometric of the test section coordinate axis -----	66
22.	Velocity profiles at the test section entrance, plate leading edge, and the top of the cylinder for $d/r = 0.0$ -----	67
23.	Velocity profiles at the top and bottom of the cylinder for $d/r = 5.33$ -----	68

ACKNOWLEDGMENT

I would like to thank all of the people involved in the support of this work, clerical and technical; but it is with special appreciation that I thank Professor Mathew Kelleher, Mr. George Bixler, and Mr. Thomas Christian for their guidance and assistance.

I would also like to thank my advisor, Professor Thomas E. Cooper, whose professionalism, knowledge, and encouragement were inspirations to me.



I. INTRODUCTION

The principal objective of this work has been to design, construct and test an experimental apparatus which will allow the study of the influence of ground effects on a heated cylinder placed in a crossflow of air. Previous work of this nature has concentrated primarily on free cylinders. Recently, McComas (1) investigated the pressure and heat transfer characteristics of a heated cylinder attached to a wall. McComas determined the local and average Nusselt number, and the pressure coefficient, on the surface of the cylinder for Reynolds numbers varying from 53,000 to 153,000. This work is a follow-on study of the project initiated by McComas, differing in that the apparatus has been designed and constructed such that the plane surface can be varied from the attached position to approximately 3 cylinder diameters away. Due to the limitations of the wind tunnel used by McComas, (described in detail in (1)), hotwire anemometry and flow visualization techniques were not able to be used in his investigations. The present experimental apparatus is located in the Mechanical Engineering Department wind tunnel in Building 500 on the Naval Postgraduate School campus. This wind tunnel, described in detail in section III, has a speed range of 10 to 175 miles per hour, and is equipped with a traversing mechanism and hotwire anemometer which can be used to obtain velocity information throughout the test



section. The tunnel also has a capability for flow visualization using smoke filaments.

Experiments were conducted at a free stream Reynolds number of 153,000 for cylinder to plate spacings of $d/r = 0.0, 0.25, 0.5, 1.0, 2.0, 4.0, 5.33$ (maximum separation) where d = gap width and r = cylinder radius (Figure 1). The flow field in the vicinity of the cylinder was probed using the hot wire anemometer. The velocity distribution suggested that flow blockage was a factor in the experiment, and that the Reynolds number should be based on a corrected free stream velocity. The correction produced an effective Reynolds number of 161,000. Using this corrected Reynolds number, the data taken at $d/r = 0.0$ agrees with the results of McComas, and the data at $d/r = 5.33$ agrees with the work of Field (2).

As was the case with McComas, experiments with the cylinder attached to the plate showed a critical flow pattern to exist over the top half of the cylinder. As the cylinder to plate spacing was increased, this flow pattern changed from critical to subcritical over a narrow range of plate spacing (at about $d/r = 0.09$). The flow over the bottom half of the cylinder exhibited critical flow as soon as a space existed. This flow also changed from critical to subcritical, but the change was less pronounced and it was at a larger cylinder to plate spacing (at about $d/r = 1.2$).



Determination of d/r

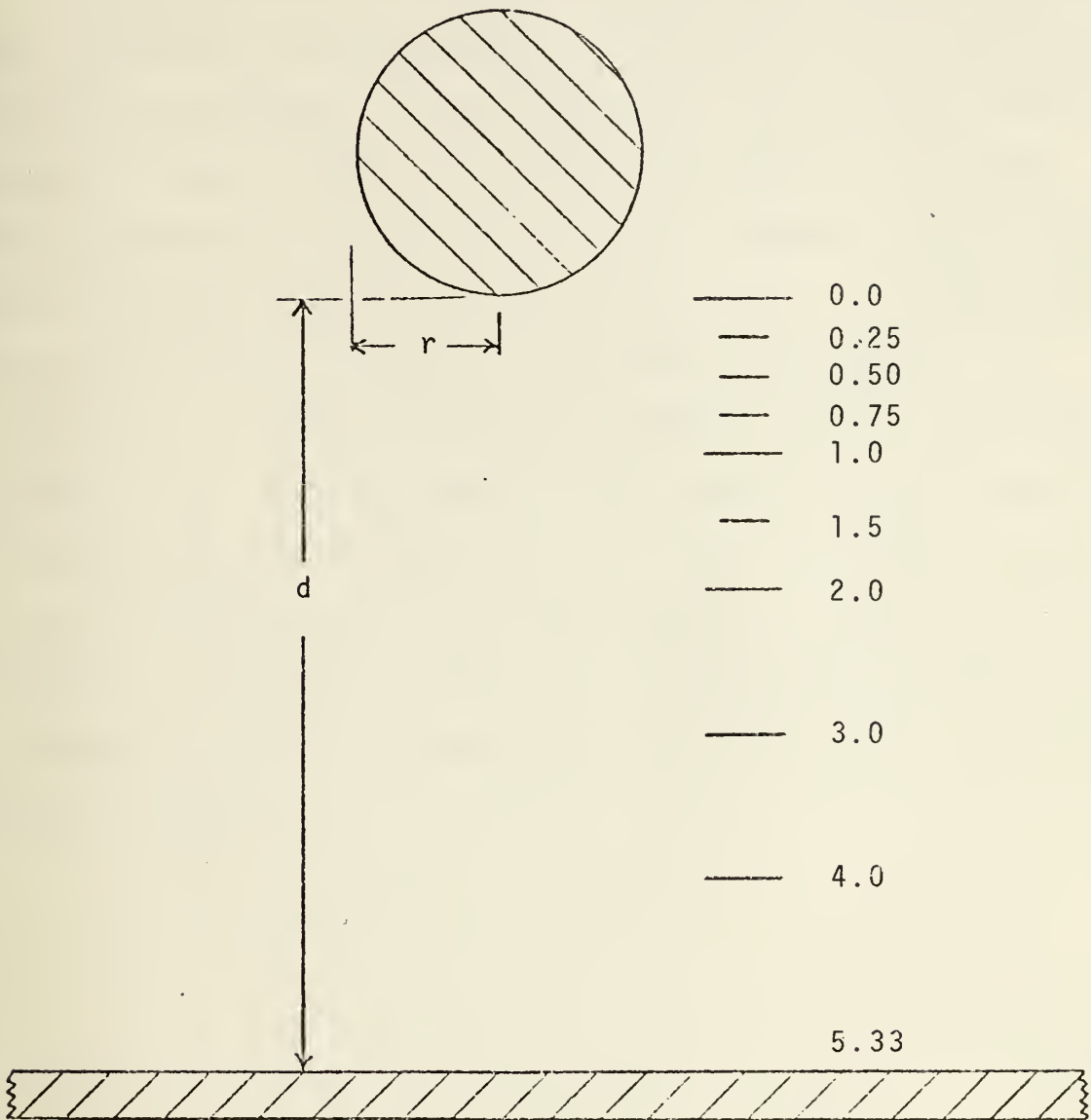


Figure 1. Schematic diagram showing determination of d/r .



Another phenomenon which was seen to occur with increasing d/r was the gradual shift of the stagnation and laminar separation points over a range of 15 to 20 degrees.

In calculating and plotting the average Nusselt number as a function of gap spacing, an interesting and unexpected trend was revealed. It was found that the minimum average Nusselt number did not occur when the plate was attached to the cylinder, but at a $d/r = 0.25$. Further, this curve also indicated a maximum point at $d/r = 2.0$. Although the current data are incomplete, (further investigation is needed over a range of Reynolds numbers) the \overline{Nu} versus d/r curve at $Re = 153,000$ suggests that gap spacing may exert a strong influence on the behavior of the flow field. Future studies employing both flow visualization as well as heat transfer measurements would aid in establishing a plausible explanation for the trends observed in the curve of average Nusselt numbers.



II. BACKGROUND

Although a great deal of investigation has been devoted to the flow and heat transfer characteristics of cylinders far from boundaries, see Meyer (5) and Field (2) for a list of references, virtually no references have been found relating to the heat transfer and flow characteristics of a cylinder placed in close proximity to a plane surface. The practical applications of such information would extend from aiding in conducting thermal analysis of container stored ordnance, rockets and missiles to the determination of the optimum size and spacing for heat exchanger tubes.

Although McComas (1) experimentally determined local and average heat transfer coefficients on the surface of a uniformly heated cylinder attached to a wall, McComas found no references to either theoretical or experimental work on this subject. McComas proposed a theory, based on theories that had been postulated for forward and rear facing steps, that quantitatively explained the trends in his heat transfer data. Other than McComas' work, no further references have been found dealing with attached cylinders.

Since the fluid flow field and thermal field are intimately coupled in a forced convection process, an understanding of the flow field is mandatory if one is to understand the heat transfer process. A thorough discussion of the fluid flow and heat transfer characteristics of a free

MEMORANDUM

TO THE PRESIDENT

FROM THE SECRETARY

1. The following information was received from the Department of the Interior on the 10th inst. regarding the proposed construction of a dam across the Colorado River at the mouth of the Grand Canyon. The project is being considered by the Department of the Interior and the Department of War, and the Department of the Interior is now in the process of preparing a report on the subject.

2. The proposed dam is to be located at the mouth of the Grand Canyon, and is to be a concrete dam, 1,000 feet high, and 1,000 feet wide at the base. The dam is to be constructed on the Colorado River, and is to be a concrete dam, 1,000 feet high, and 1,000 feet wide at the base. The dam is to be constructed on the Colorado River, and is to be a concrete dam, 1,000 feet high, and 1,000 feet wide at the base.

3. The dam is to be constructed on the Colorado River, and is to be a concrete dam, 1,000 feet high, and 1,000 feet wide at the base. The dam is to be constructed on the Colorado River, and is to be a concrete dam, 1,000 feet high, and 1,000 feet wide at the base. The dam is to be constructed on the Colorado River, and is to be a concrete dam, 1,000 feet high, and 1,000 feet wide at the base.

4. The dam is to be constructed on the Colorado River, and is to be a concrete dam, 1,000 feet high, and 1,000 feet wide at the base. The dam is to be constructed on the Colorado River, and is to be a concrete dam, 1,000 feet high, and 1,000 feet wide at the base. The dam is to be constructed on the Colorado River, and is to be a concrete dam, 1,000 feet high, and 1,000 feet wide at the base.

5. The dam is to be constructed on the Colorado River, and is to be a concrete dam, 1,000 feet high, and 1,000 feet wide at the base. The dam is to be constructed on the Colorado River, and is to be a concrete dam, 1,000 feet high, and 1,000 feet wide at the base. The dam is to be constructed on the Colorado River, and is to be a concrete dam, 1,000 feet high, and 1,000 feet wide at the base.

6. The dam is to be constructed on the Colorado River, and is to be a concrete dam, 1,000 feet high, and 1,000 feet wide at the base. The dam is to be constructed on the Colorado River, and is to be a concrete dam, 1,000 feet high, and 1,000 feet wide at the base. The dam is to be constructed on the Colorado River, and is to be a concrete dam, 1,000 feet high, and 1,000 feet wide at the base.

7. The dam is to be constructed on the Colorado River, and is to be a concrete dam, 1,000 feet high, and 1,000 feet wide at the base. The dam is to be constructed on the Colorado River, and is to be a concrete dam, 1,000 feet high, and 1,000 feet wide at the base. The dam is to be constructed on the Colorado River, and is to be a concrete dam, 1,000 feet high, and 1,000 feet wide at the base.

8. The dam is to be constructed on the Colorado River, and is to be a concrete dam, 1,000 feet high, and 1,000 feet wide at the base. The dam is to be constructed on the Colorado River, and is to be a concrete dam, 1,000 feet high, and 1,000 feet wide at the base. The dam is to be constructed on the Colorado River, and is to be a concrete dam, 1,000 feet high, and 1,000 feet wide at the base.

9. The dam is to be constructed on the Colorado River, and is to be a concrete dam, 1,000 feet high, and 1,000 feet wide at the base. The dam is to be constructed on the Colorado River, and is to be a concrete dam, 1,000 feet high, and 1,000 feet wide at the base. The dam is to be constructed on the Colorado River, and is to be a concrete dam, 1,000 feet high, and 1,000 feet wide at the base.

10. The dam is to be constructed on the Colorado River, and is to be a concrete dam, 1,000 feet high, and 1,000 feet wide at the base. The dam is to be constructed on the Colorado River, and is to be a concrete dam, 1,000 feet high, and 1,000 feet wide at the base. The dam is to be constructed on the Colorado River, and is to be a concrete dam, 1,000 feet high, and 1,000 feet wide at the base.

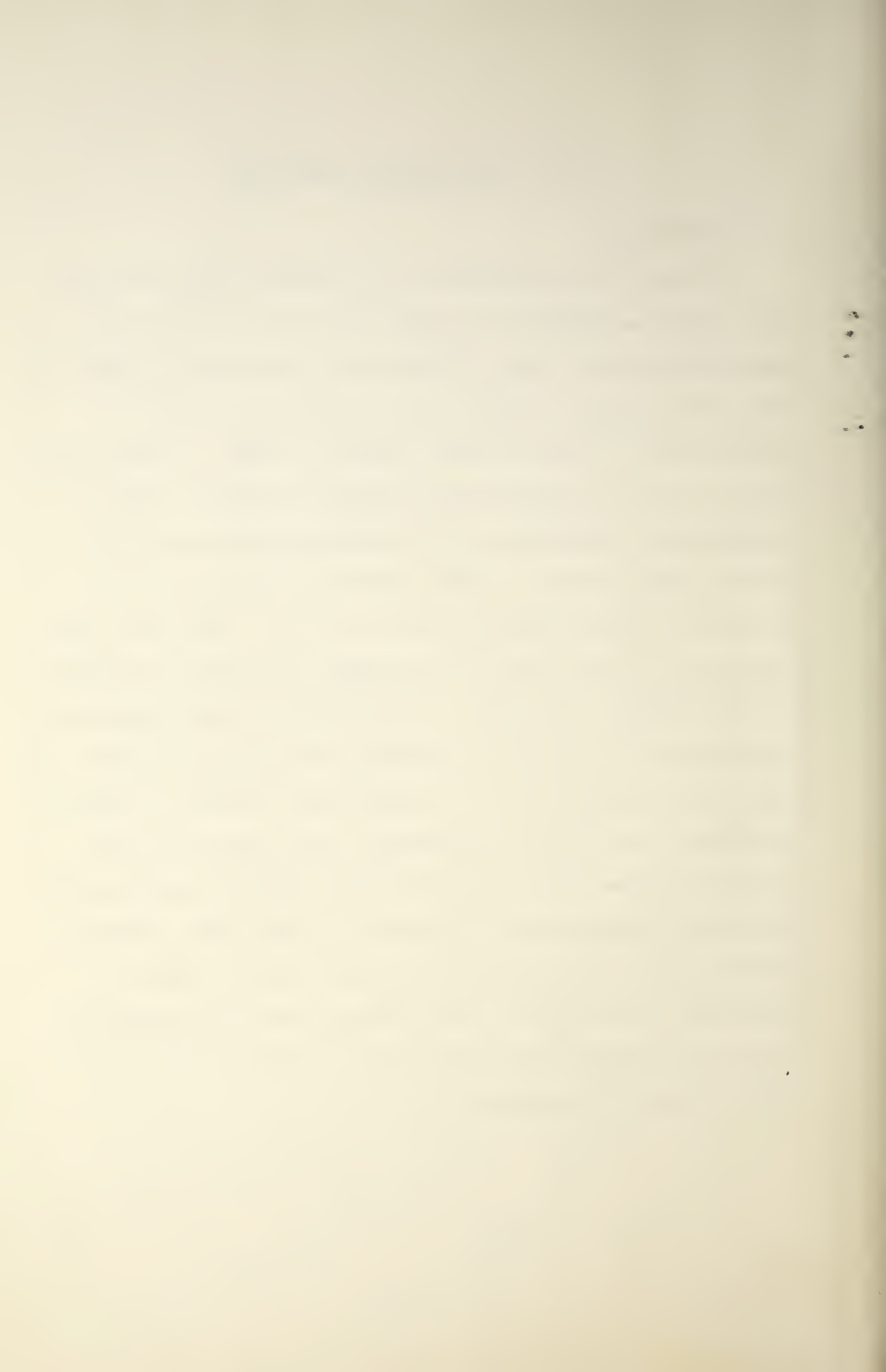
cylinder can be found in (3), and a proposed but as yet unverified description of the flow around an attached cylinder can be found in (1).



III. EXPERIMENTAL APPARATUS

A. WIND TUNNEL

All tests were conducted in a subsonic, open circuit, wind tunnel manufactured to Navy specifications by the Kenny Engineering Corp., of Monrovia, California (Figure 2). The overall length of the tunnel was 40 feet, with an entrance bell 5 feet, 5 inches wide by 7 feet, 5 inches high. The test section was 20 inches wide by 28 inches high at the entrance, expanding to 31 inches high to allow for boundary layer growth. These dimensions resulted in a contraction ratio, based on area, of 10:1. The tunnel was powered by a 75 HP, 1750 rpm variable speed motor driving a 45 inch diameter adjustable pitch vaneaxial fan capable of supplying air at 10,000 to 70,000 cubic feet per minute. The tunnel was equipped with six graded mesh screens to control turbulence and a 24 inch manometer tube tapped into the stilling chamber and test section for velocity measurement. The tunnel was designed to operate at velocities ranging from 10 mph (14.67 ft/sec) to 175 mph (256.67 ft/sec). Turbulence intensity was taken using a hot wire anemometer and found to be approximately 0.2% at a free stream velocity of 98 ft/sec (see Appendix D).



OPEN CIRCUIT SUBSONIC WIND TUNNEL

Bldg. 500
Naval Postgraduate School
SCALE: 1 in = 5 ft

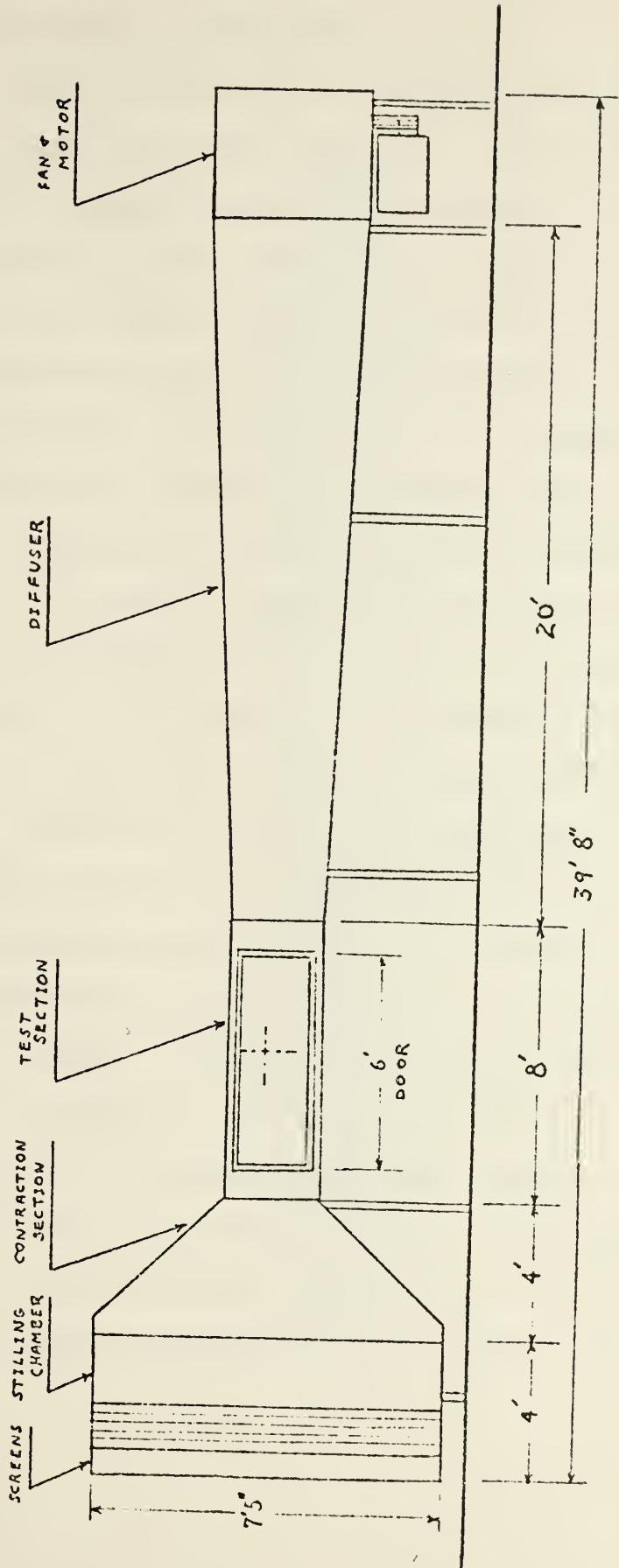


Figure 2. Schematic diagram of the wind tunnel.

B. HEAT TRANSFER EXPERIMENT

The test cylinder was essentially three cylinders attached end to end (see Figure 3). The two end sections were hollow softwood cylinders supported by a hardwood brace, curved to match the cylinder contour. The central cylinder was a sheet of resistive paper (Temsheet) fitted into stepped portions of the end cylinders, and attached to the end cylinders and hardwood brace by double sided adhesive tape. The three cylinders then formed one cylinder 20 inches long, to correspond to the test section width, and having a diameter of 3 inches, chosen to allow maximum resolution of the liquid crystals without excessive blockage within the test section. The assembled test cylinder was tightly packed with glass wool to minimize heat transfer into the cylinder, and thereby reduce the time needed to reach steady state after a voltage was applied to the paper.

The resistive paper used was a commercially available, carbon impregnated paper, Temsheet, with a nominal thickness of 0.039 inches. The width was sized to conform to the stepped circumference of the end cylinders (9.422 inches) and the length was 12 inches. The circumference of the resistive paper cylinder was marked in 5 degree increments, in two locations 2 inches apart. This was the test section used in all heat transfer experiments. The entire outer surface of



Figure 3. Photograph of the Tensheet cylinder.

the resistive paper was covered with three coats of NCR S-43 liquid crystals having event temperatures of:

red: 109.8°F
green: 111.0°F
blue: 112.3°F (Field (2))

Power was applied to the paper by means of wires lead inside the cylinder through one end. The wires were attached to aluminum foil tape by means of alligator clips, and the edges of the tape were painted with silver paint to assure good electrical contact with the paper. The nominal distance between the tape/paint was 4.8125 inches, resulting in a surface area for power dissipation of 45.34 in².

The power source used was a Lambda regulated power supply, model LK 345A FM. The voltage applied by the Lambda was measured by a Fluke 8100A digital multimeter. This multimeter was also used to measure the resistance of the resistive paper. Air stream temperature was sensed by a copper-constantan thermocouple installed in the stilling chamber. The thermocouple output was read on a Leeds & Northrup millivolt potentiometer.

The "wall" used in these experiments was manufactured from 1/2 inch plexiglass. This plate was 46 inches long, the maximum practical length, to minimize the influence of the trailing edge on the flow patterns around the cylinder. The width of the plate was 20 inches, to conform to the test section width, and it was beveled on the under side of the leading edge at an angle of approximately 12 degrees.

The plate and cylinder were placed in the tunnel horizontally, and in such a way that the leading edge of the plate extended four cylinder diameters (12 inches) ahead of the cylinder centerline. The cylinder was attached to the test section walls by portions of the end cylinders protruding through holes cut for that purpose. The plate was capable of being moved vertically by means of a threaded rod extending through the tunnel floor, and a rear brace which locked in position by means of a split nut (Figure 4). The plate was capable of being located at any position relative to the cylinder, from attached, to a maximum possible distance of 8 inches away (Figure 1).

C. PRESSURE COEFFICIENT EXPERIMENT

The experiments conducted to find the variation of pressure around the circumference of the cylinder used the previously described plexiglass plate as the wall and a 3 inch diameter aluminum cylinder fitted with four pressure taps 90 degrees apart (Figure 5). The circumference of the cylinder was scribed in 5 degree increments. Plastic tubing led from the taps through one end of the cylinder to a manometer bank.

The manometer bank consisted of several tubes that were inclined at an angle of 30 degrees from the vertical. All four cylinder pressure taps as well as the stilling chamber and test section pressures were read from this manometer bank.

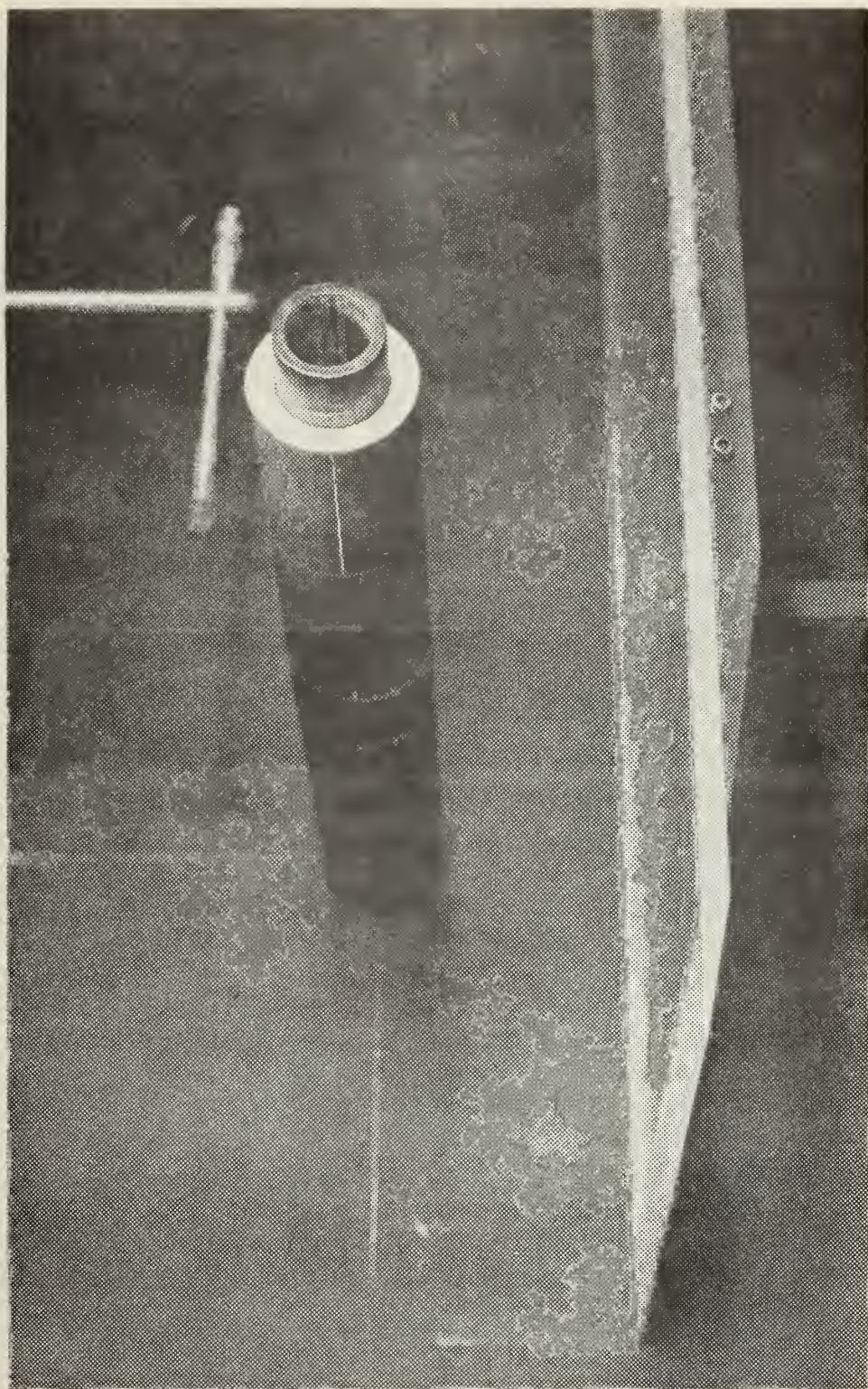


Figure 4. Photograph of the plate and cylinder assembly.

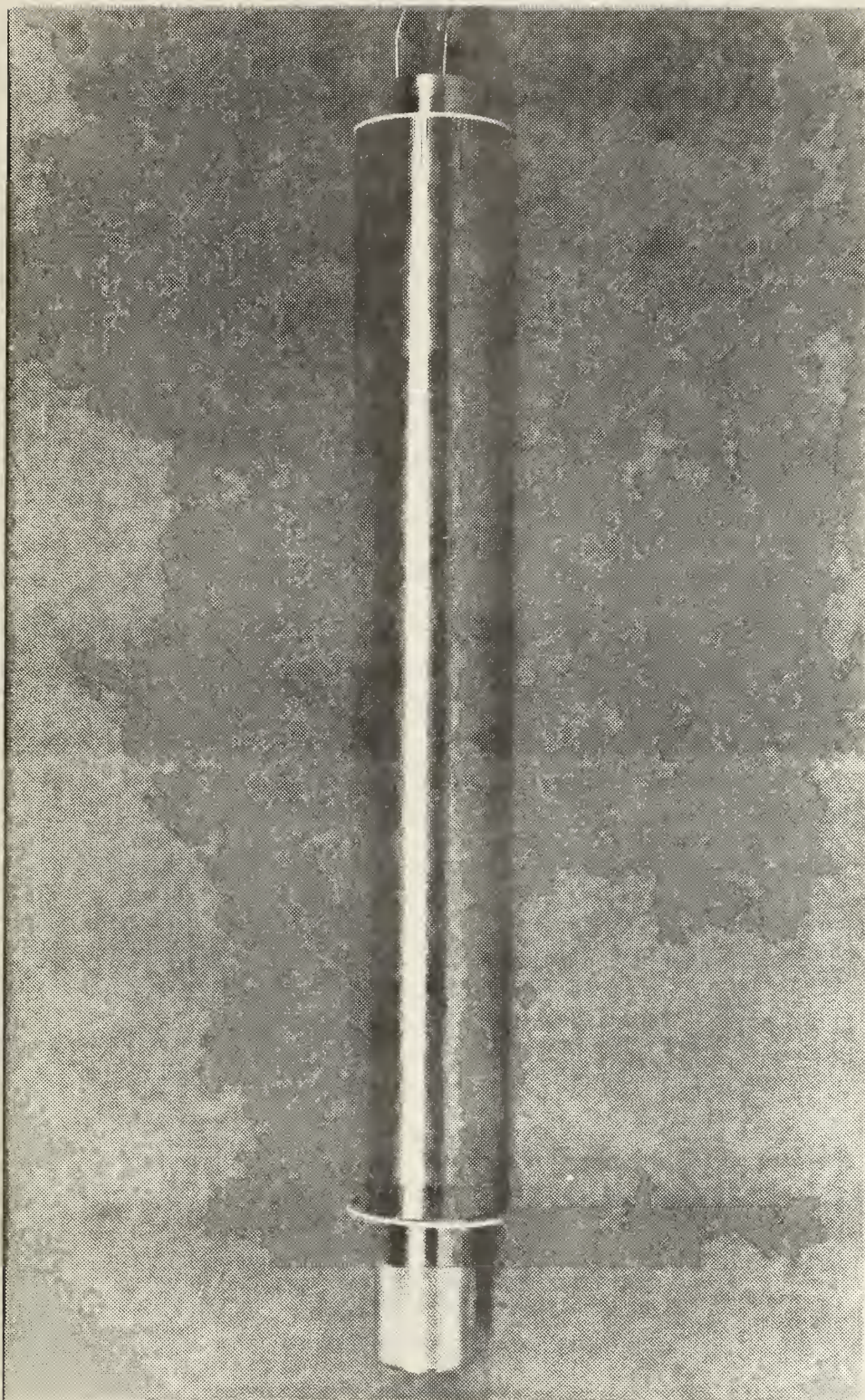


Figure 5. Photograph of the cylinder used to collect pressure data.

IV. EXPERIMENTAL PROCEDURE

The present work was conducted utilizing different test facilities than those used in previous investigations. The wind tunnel was smaller, and of the open circuit variety. Due to experimental considerations, the cylinder size and orientation were different, and the problem of varying the relative separation of the plate and cylinder was unique to this work. In order to assure that meaningful and accurate data would be obtained, it was necessary to compare initial results with previous work. Since both Field and McComas performed experiments at a Reynolds Number of 153,000, it was decided to check the present apparatus at that Reynolds Number. For this reason, an air stream speed of 98 ft/sec was used for comparison experiments. Because of time limitations, all of the data for the present work were taken at 98 ft/sec, corresponding to a Reynolds Number of 153,000, where Reynolds number is defined as:

$$Re = \frac{U_{\infty} d}{\nu}$$

Re = Reynolds number

U_{∞} = free stream velocity at test section entrance, ft/sec

d = cylinder diameter, ft

ν = kinematic viscosity of air, ft²/sec

A. HEAT TRANSFER EXPERIMENT

The same experimental procedure used by Field and McComas was used in the present experiments. For completeness, a description of the procedures will be repeated here.

Prior to the start of the experiment a sufficient voltage was applied to the cylinder to cause the liquid crystals to reach their event temperature and change color. This voltage was usually from 12 to 15 volts. After about a half hour, time to allow the cylinder and glass wool packing to come to a steady state temperature, the power supply was turned off and the multimeter was switched from DC voltmeter to ohmmeter. In this manner an accurate value of the paper resistance was determined at a temperature which corresponded to the liquid crystal event temperature. The multimeter was then switched back to DC voltmeter and the wind tunnel was started and brought up to speed.

The wind tunnel velocity range and test section velocity profile were examined prior to obtaining experimental heat transfer data (see Appendix D). It was determined that the velocity profile was uniform at the test section entrance, and that the turbulence intensity was approximately 0.2%. After numerous checks with the hot wire anemometer, it was decided to use the installed wall manometer to set the tunnel speed of 98 ft/sec.

After the tunnel reached operating speed, the voltage was adjusted such that the liquid crystal color bands would appear at various angular positions around the cylinder. The first color band to appear would be at the lowest local Nusselt number on the cylinder. For tests with a d/r greater ^a than 0.25 (where d = distance from plate to cylinder rim, and r = cylinder radius) this was always the laminar separation point (Figures 13-19). As voltage was increased, the color lines would appear in one, or as many as 5 or 6, angular locations all having equal Nusselt numbers. In this manner the cylinder surface temperature could be compared to the air stream temperature as determined by a thermocouple mounted in the wind tunnel stilling chamber. Using this temperature difference, and calculating the power dissipated from the voltage applied, the local heat transfer coefficient could be calculated for the circumference of the cylinder. Because of the way the cylinder was constructed, readings within 15 degrees of the seam were considered unreliable. The majority of Nusselt number data were collected with the seam located at 180 degrees. The Nusselt number in the vicinity of 180 degrees was determined by turning the cylinder such that the seam was facing forward at 0 degrees. Several experiments were also made with the seam at positions of 135, 225, and 315 degrees. The final position of 0 degrees was chosen for the seam after it was observed that the value and angular location of the Nusselt number at the laminar

separation point, and in the vicinity of 130 and 210 degrees, was consistent with the values obtained with the seam at 180 degrees.

For all experiments, distinct, repeatable values of the Nusselt number versus angular location were obtained. The gradient as determined by the color bands, was sharp, with the exception of a region near the forward stagnation point, which appeared nearly isothermal. The gradient was also indistinct in the turbulent boundary layer, where the "scrubbing" action of cooler air caused the Nusselt number to change with time. Therefore, the Nusselt number shown for the turbulent regions must be considered to be an average value.

B. PRESSURE COEFFICIENT EXPERIMENT

With the pressure cylinder mounted in the wind tunnel, the manometer bank was leveled, pressure leads checked for tightness, and the wind tunnel brought up to a speed of 98 ft/sec, corresponding to a Reynolds number of 153,000. The cylinder was positioned such that the pressure taps were initially at 0, 90, 180, and 270 degrees. The manometer readings for the four taps, the stilling chamber, and the test section were recorded. The cylinder was rotated in 5 degree increments until pressure readings were obtained for the entire circumference.

The pressure coefficient was determined as follows:

$$C_p = \frac{P - P_\infty}{\frac{1}{2}\rho U_\infty^2} = \frac{P - P_\infty}{P_s - P_\infty}$$

where: C_p = pressure coefficient
 ρ = density of air
 U_∞ = air stream velocity (test section entrance)
 P = pressure on cylinder surface
 P_s = stagnation pressure (stilling chamber)
 P_∞ = air stream static pressure (test section entrance)

V. RESULTS

Initial heat transfer and pressure coefficient experiments were made with the plate and cylinder attached ($d/r = 0.0$). A thin felt strip was placed between the two to assure a tight seal. The data obtained in this configuration agreed well with the results of McComas (see Figure 6). It can be seen that the trends in the data are identical, that local maximum and minimum values are within experimental uncertainty (see Appendix B for uncertainty analysis), and that a local maximum and local minimum were again observed near the point of attachment of the plate and cylinder. This is further evidence of the trapped vortex phenomenon as proposed by McComas.

The next series of tests were made with the plate as far removed from the cylinder as possible, $d/r = 5.33$, or $d = 8$ inches. As there appeared to be some blockage, the method of Pope (4), as used by Meyer (5), was used to determine the necessary correction:

$$Re_{corr} = (1.0 + e)Re_{\infty}$$

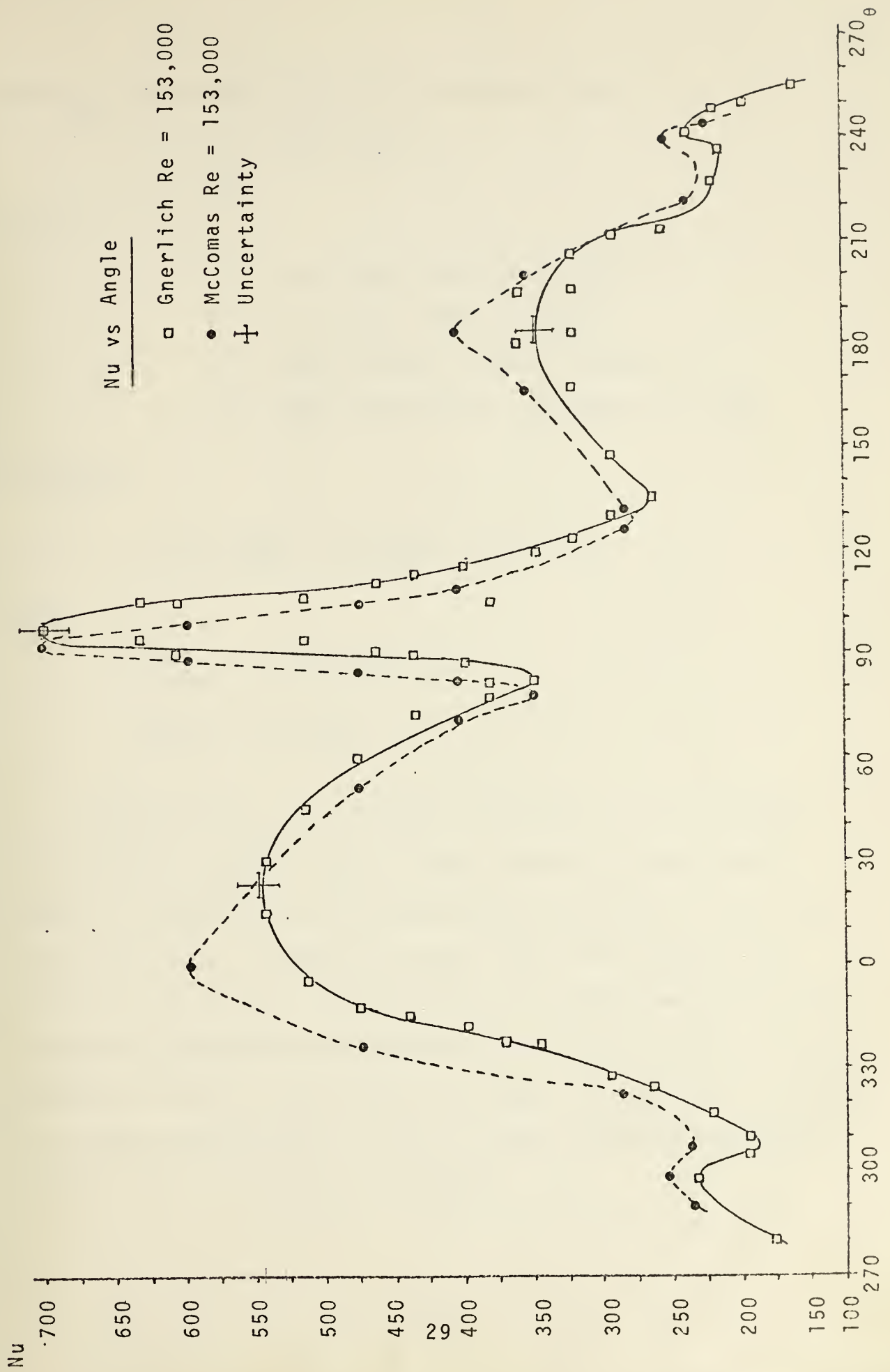
where:

$$e = e_{sb} + e_{wb}$$

and e_{sb} is the solid blockage correction factor:

$$e_{sb} = \frac{\pi^2}{3} \left(\frac{r}{H} \right)^2$$

Figure 6. Comparison of the heat transfer results for $d/r = 0.0$ with the results of McComas at $Re = 153,000$.



and e_{wb} is the wake blockage correction factor:

$$e_{wb} = 1/4 (D/H) C_D$$

where:

D = cylinder diameter, inches

r = cylinder radius, inches

H = total tunnel height, inches

C_D = drag coefficient (see Meyer p. 107)

Therefore:

$$e = \frac{2}{3} \left(\frac{1.5}{24} \right)^2 + \frac{1}{4} \left(\frac{3}{24} \right) (1.2) = 0.05$$

and:

$$Re_{corr} = (1.05) 153,000$$

$$Re_{corr} = 161,000$$

Using the Re_{corr} to compare the results of this experiment with the work of Field, it was found that the results compare favorably with Field and with the theory of Schuh (6) (see Figure 7). It should be noted that Field experienced critical flow at $Re = 149,000$, while the experiments made in this work were exclusively subcritical for $d/r = 5.33$. This phenomenon could be attributed to higher free stream turbulence or cylinder deformation, either of which could have induced critical flow in Field's experiments.

$\frac{Nu}{\sqrt{Re}}$ vs Angle

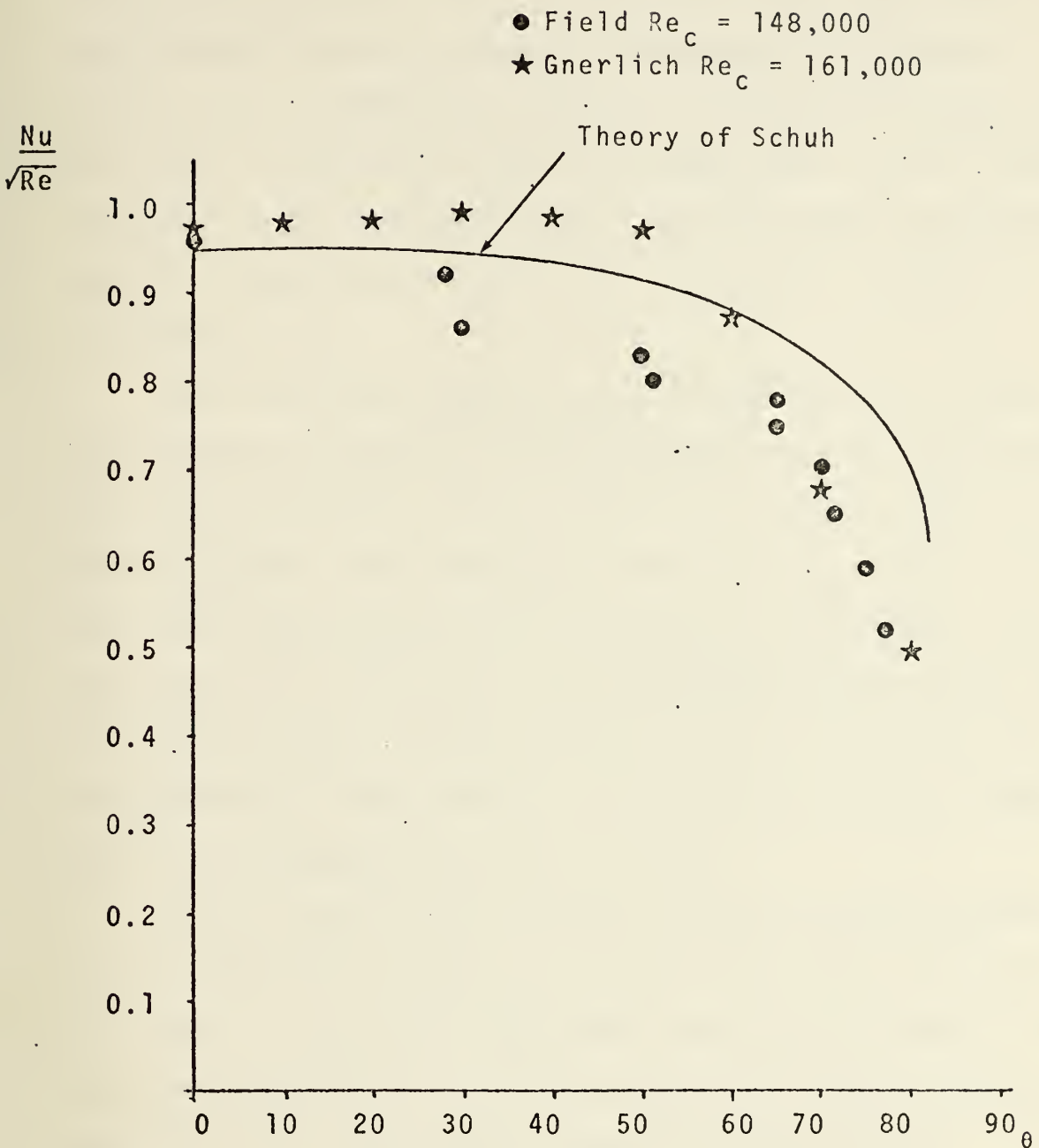


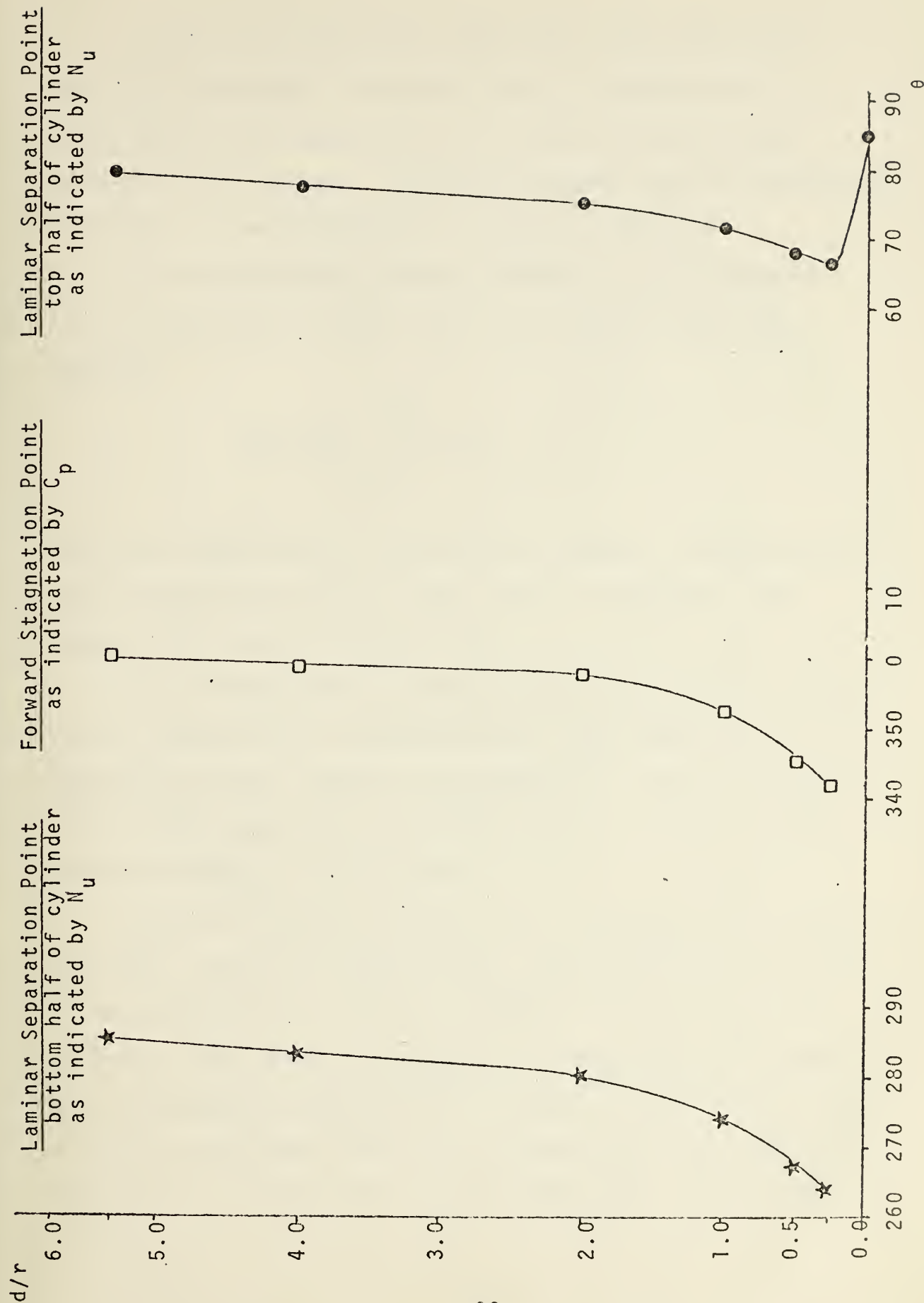
Figure 7. Comparison of the heat transfer results for $d/r = 5.33$ and $Re_{corr} = 161,000$ with the results of Field at $Re = 148,000$ and with the theory of Schuh

Figures 13 through 19 are polar plots of the local Nusselt number and pressure coefficient for values of d/r ranging from 0.0 to 5.33. In examining the seven plots for significant trends or unusual phenomena, two items of interest were immediately apparent: one was the change from critical to subcritical flow, the other was a shift in the location of the stagnation point and the laminar separation points as the plate was moved away from the cylinder (see Figure 8).

The transition from critical to subcritical flow was investigated in order to ascertain the d/r ratio associated with the transition. As the flow was critical with the plate attached, and subcritical over the top at $d/r = 0.25$, the first transition point of interest was located in the interval $0.0 \leq d/r \leq 0.25$. By alternately moving the plate and adjusting the voltage, the transition point from critical to subcritical flow over the top of the cylinder was found to be approximately $0.08 \leq d/r \leq 0.10$.

As the flow over the bottom of the cylinder underwent a transition from critical to subcritical flow in the interval $1.0 < d/r < 1.5$, this region was investigated further. Using the same procedure of carefully adjusting spacing and voltage, the transition was found to occur at approximately $1.17 \leq d/r \leq 1.25$.

Figure 8. Shift of the Laminar separation points and the stagnation point with increasing d/r .



It should be noted that while both flows described above are definitely critical, there is significant difference in the degree of criticality on the top and bottom of the cylinder. This can be seen from the magnitudes of the Nu on the data shown in Figures 9 and 10.

In order to glean further information from the data, the average Nusselt number, \overline{Nu} , was computed from the equation:

$$\overline{Nu} = \frac{1}{2\pi} \int_0^{2\pi} Nu \, d\theta$$

which was numerically integrated by computer using Simpson's Rule of Quadrature with a step size of 5 degrees. The results are shown in Figure 11a.

It is interesting to note the unexpected shape of the curve. \overline{Nu} drops to a minimum value, then increases to a maximum, and then gradually decreases to a nearly constant value as d/r approaches relative infinity. These results prompted further investigation.

In order to help determine the influence of the local Nu on \overline{Nu} a plot was made of Nu_{max} for the forward (-90 to 90 degrees) and rear (90 to -90 degrees) portions of the cylinder. The results are shown in Figure 11b and exhibit the same general shape as \overline{Nu} . The drop in \overline{Nu} from $d/r = 0.0$ to 0.25 is explained from this plot when the sharp drop in Nu_{max} on the front of the cylinder from $d/r = 0.0$ to 0.25 is

$d/r = 0.0$ \times

$d/r = 0.25$ \bullet

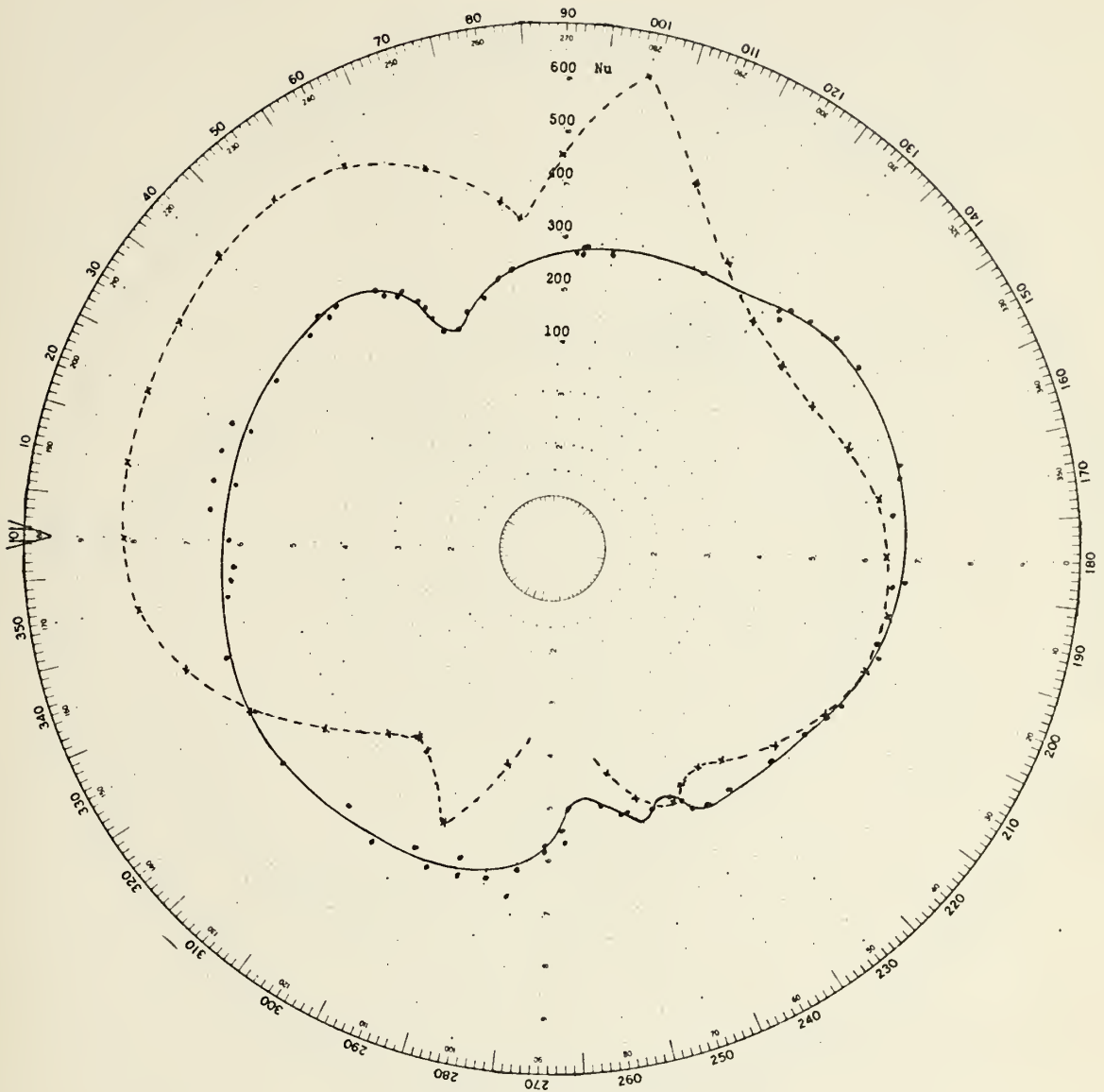


Figure 9. Comparison of the local Nusselt number at $d/r = 0.0$ with the local Nusselt number at $d/r = 0.25$.

$d/r = 0.0$ \times
 $d/r = 0.25$ \bullet

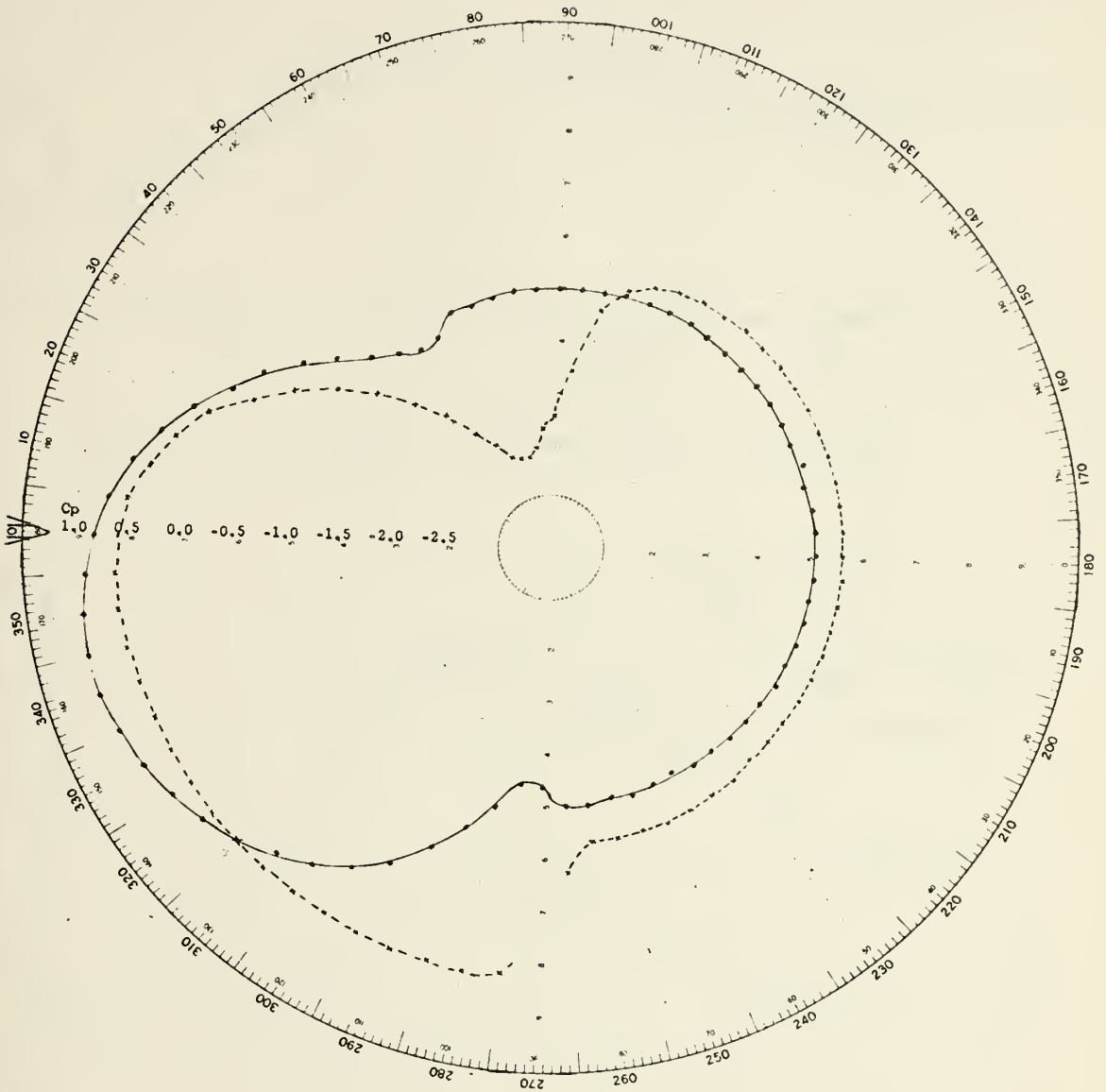


Figure 10. Comparison of the pressure coefficient at $d/r = 0.0$ with the pressure coefficient at $d/r = 0.25$.

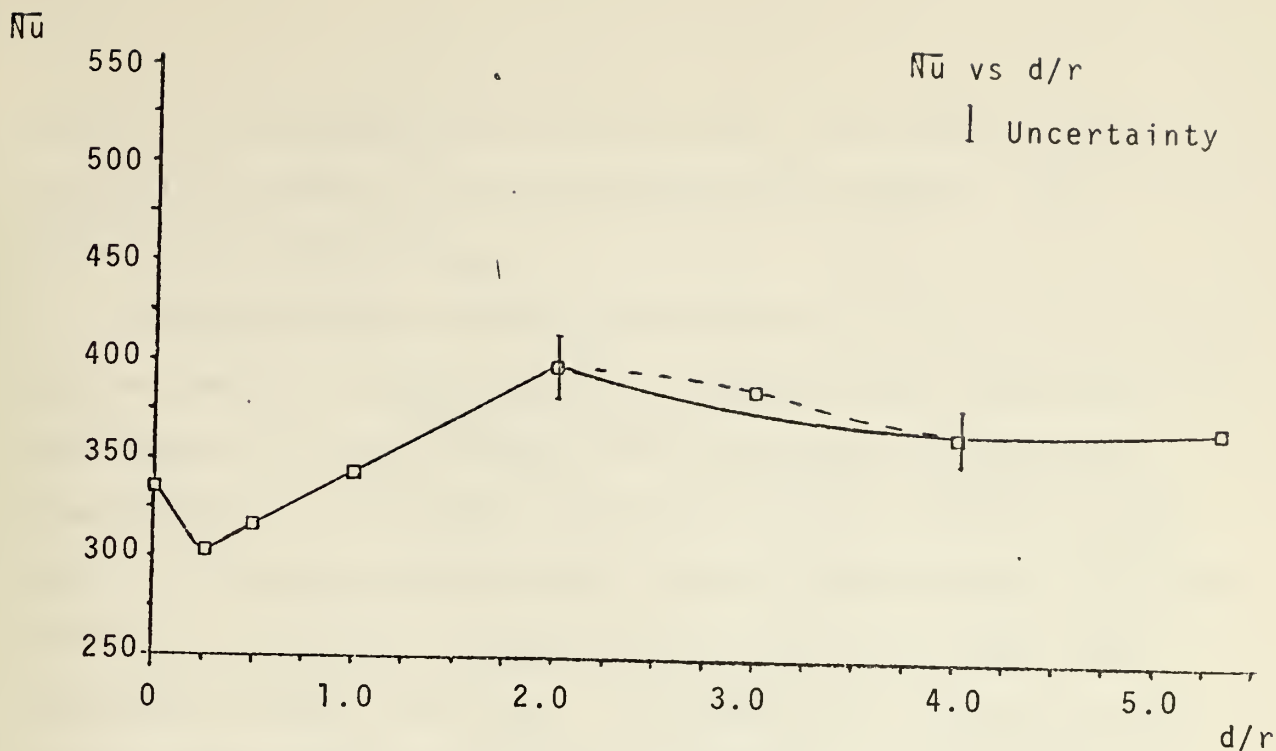


Figure 11a. Average Nusselt number versus d/r

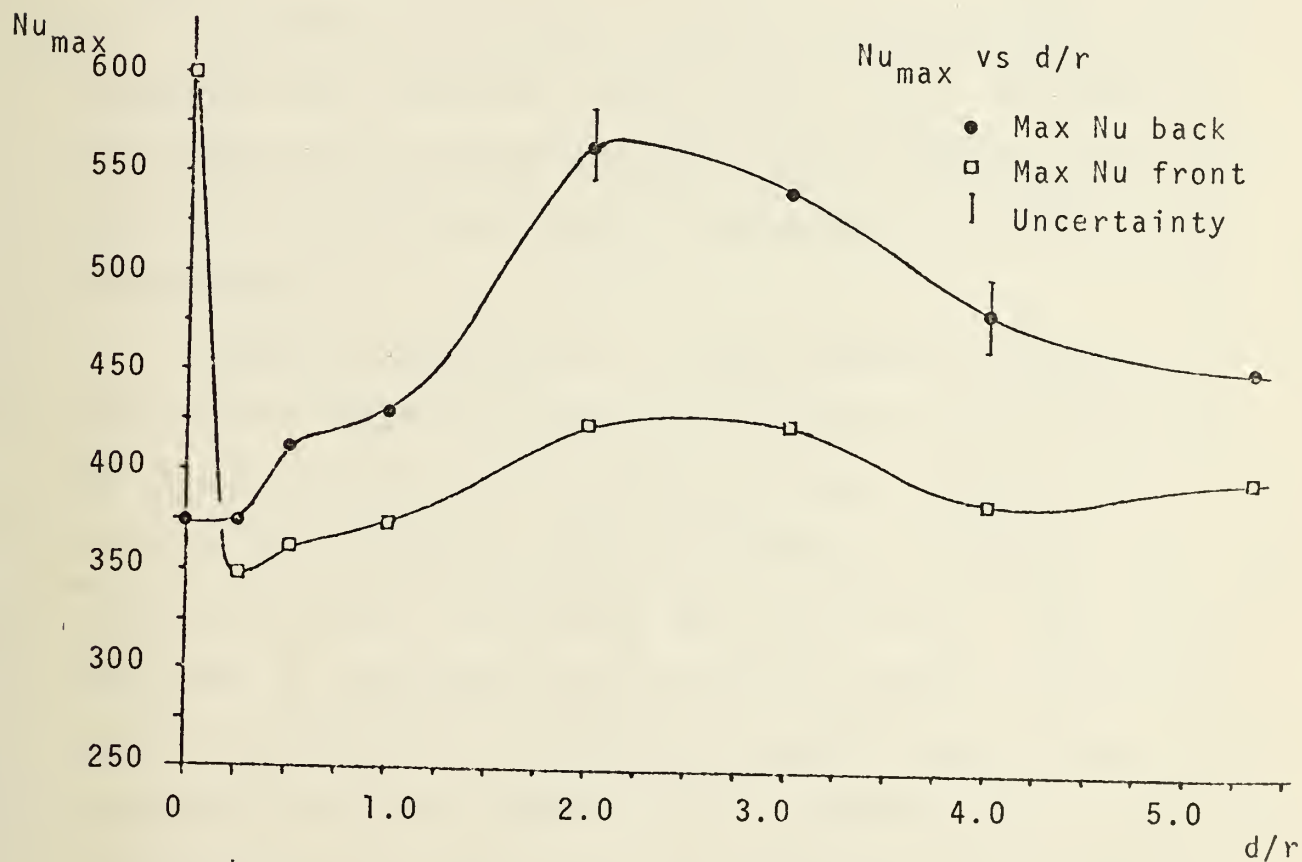


Figure 11b. Maximum Nusselt numbers on the front and back of the cylinder versus d/r .

noted. (The maximum local Nu for $d/r = 0.0$ occurs in the separation bubble, in the vicinity of 90 degrees, and is not used in the plot of Nu_{max} .)

Further investigation of the \overline{Nu} curve lead to an attempt to see how the voltage applied to the cylinder would vary if one location on the cylinder was maintained at a constant temperature as the plate spacing was varied. The locations 150 to 165 degrees were chosen for this experiment. For each d/r the voltage was adjusted until a distinct color band appeared at these locations. Plotting the voltage applied versus d/r resulted in a curve of similar shape to \overline{Nu} and Nu_{max} (see Figure 12).

In order to verify the curvature of the \overline{Nu} plot, a complete set of data was taken at $d/r = 3.0$. This data is not presented on a separate polar plot but \overline{Nu} was calculated and the value obtained enabled the shape of the \overline{Nu} curve to be verified.

A possible explanation for the observed variation in \overline{Nu} could be related to the amount of "cold" free stream air which has access to the cylinder surface. At $d/r = 0.0$, the flow is critical due to the fact that all of the air approaching the cylinder is forced to go "up and over." As soon as the plate is separated the flow has two paths. As soon as space is sufficient to provide a favorable path without large pressure gradients, enough of the air approaching the cylinder passes beneath to cause the flow over the top to transition

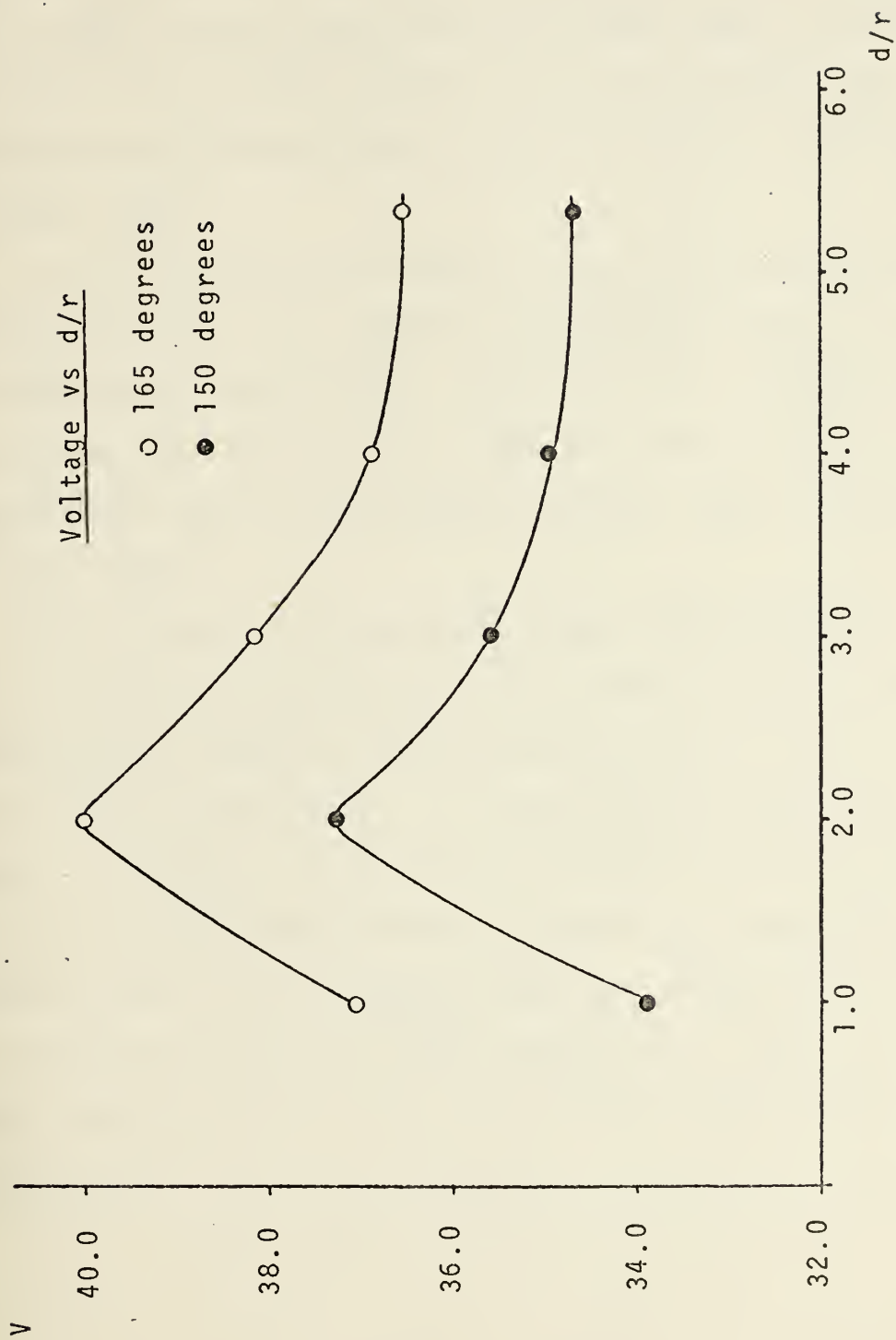


Figure 12. Voltage required to maintain a predetermined temperature at the positions of 150 and 165 degrees versus d/r .

to subcritical. Now the air passing below the cylinder is experiencing critical flow, possibly due to the nozzle effect produced by the rapidly decreasing flow area below the cylinder. The heat transfer in this region does not increase due to the fact that much air has already been heated passing over the front of the cylinder (i.e., the thermal and hydrodynamic boundary layers are a significant fraction of the gap size).

As d/r is increased beyond 0.25, the larger opening allows more cold air, outside the boundary layer, to approach the bottom of the cylinder. This cold air carries off some heat by conduction and also mixes with the warm air in the separation bubble and turbulent boundary layer, resulting in increasing \overline{Nu} .

The gradual decrease in \overline{Nu} from a high value at $d/r = 2.0$ is not understood at this time. It was expected that \overline{Nu} would approach some constant value as the influence of the plate was reduced. It can be seen from Figure 11a that the uncertainty band nearly encompasses the decrease in \overline{Nu} . Although the behavior of the Nu_{max} and voltage curves suggest that the trend may be genuine, further investigation is needed to determine if \overline{Nu} actually has a peak, or in fact approaches a constant value from some minimum point at a small d/r .

Nu •
 Cp x

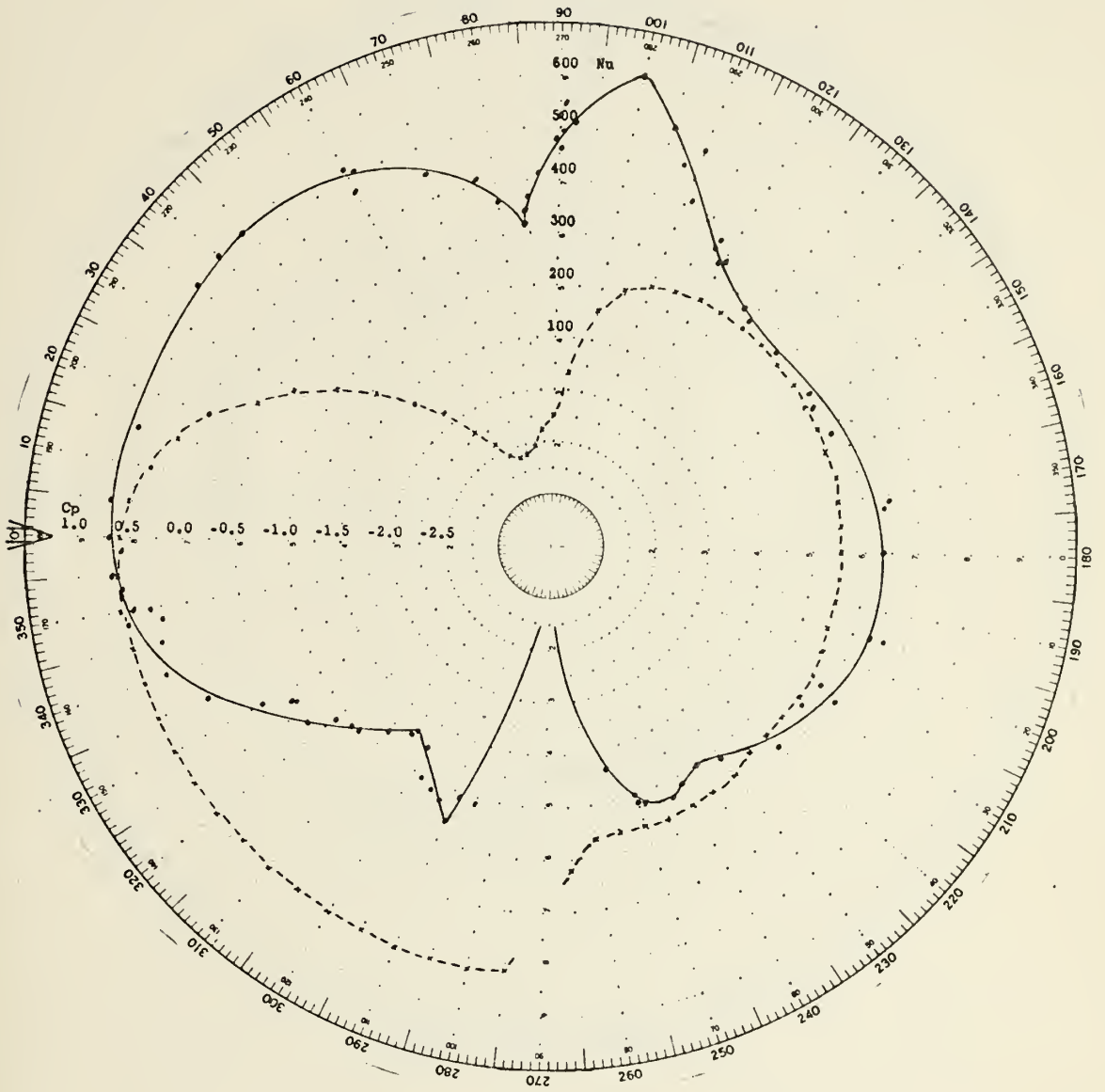


Figure 13. Polar plot of Nusselt number and pressure coefficient versus angle for $d/r = 0.0$.

Nu •
Cp x

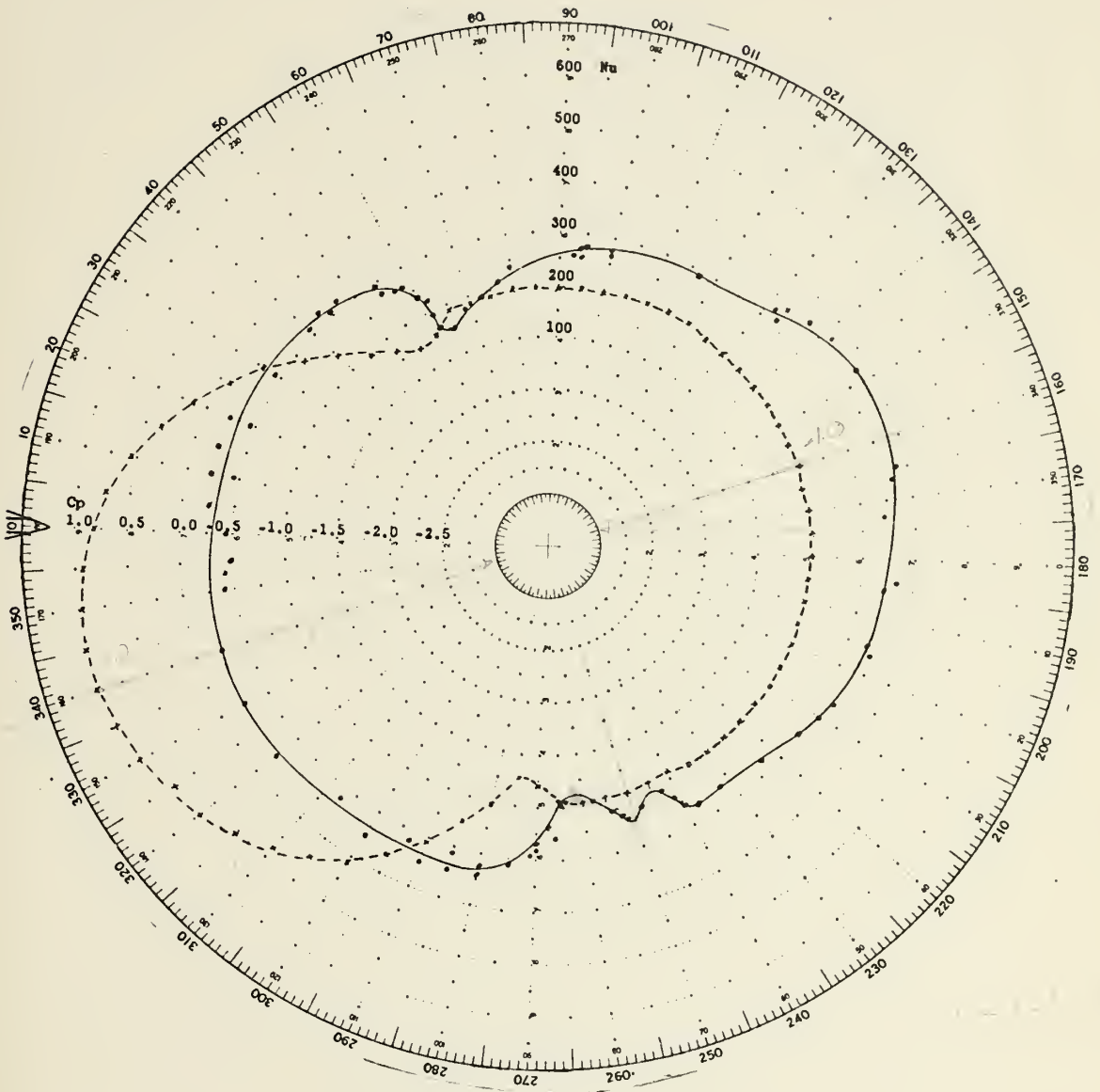


Figure 14. Polar plot of Nusselt number and pressure coefficient versus angle for $d/r = 0.25$.

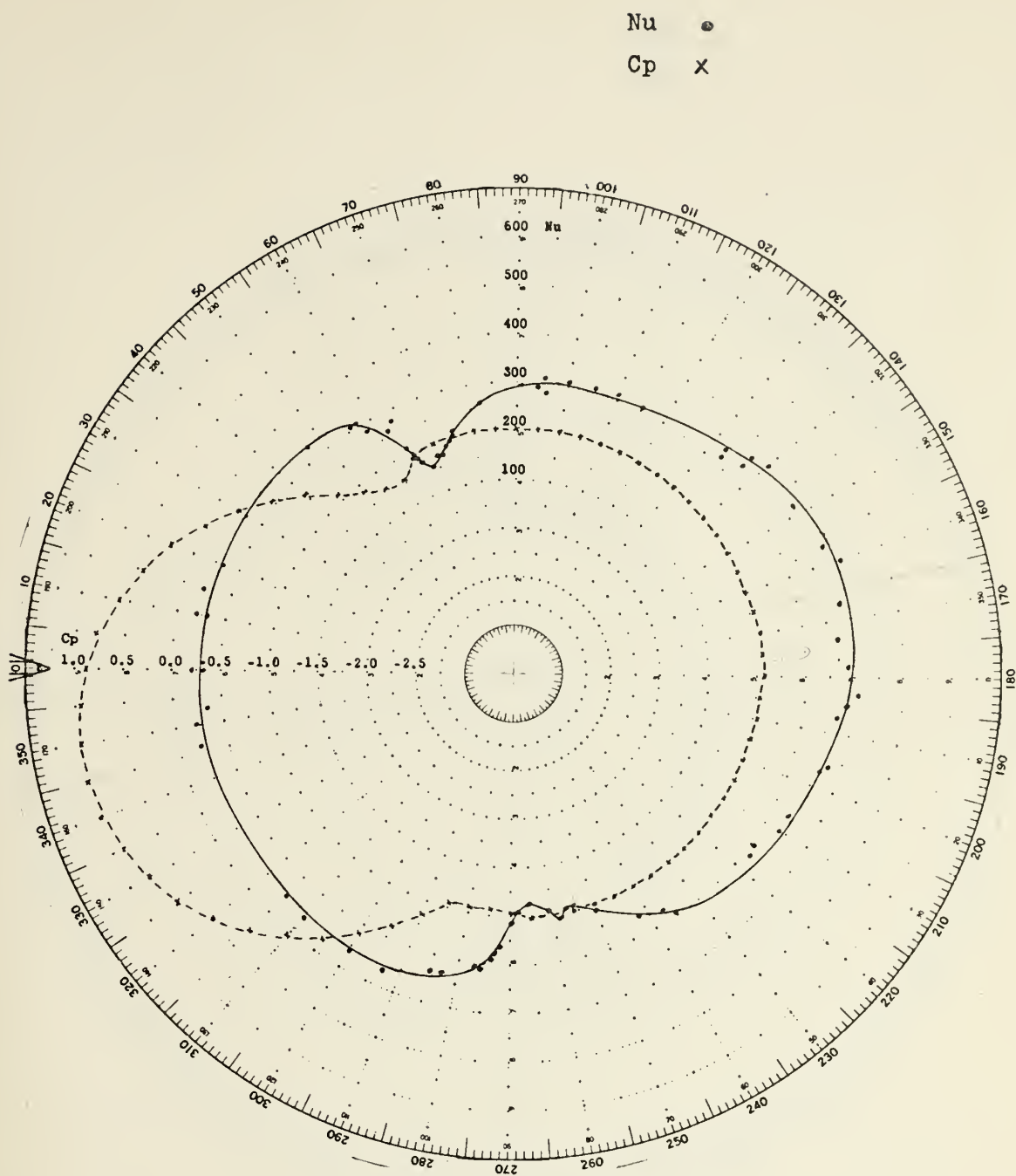


Figure 15. Polar plot of Nusselt number and pressure coefficient versus angle for $d/r = 0.5$.

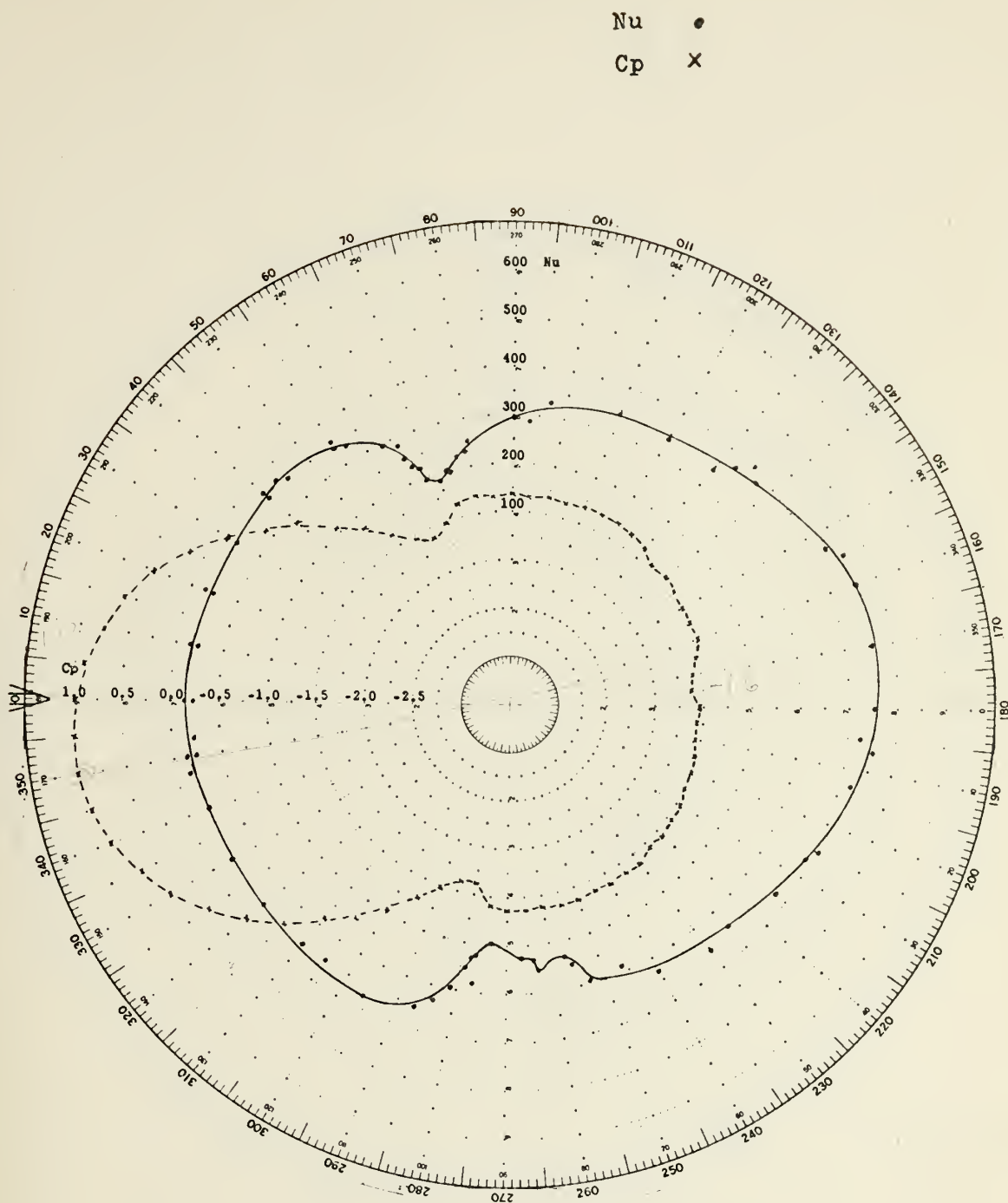


Figure 16. Polar plot of Nusselt number and pressure coefficient versus angle for $d/r = 1.0$.

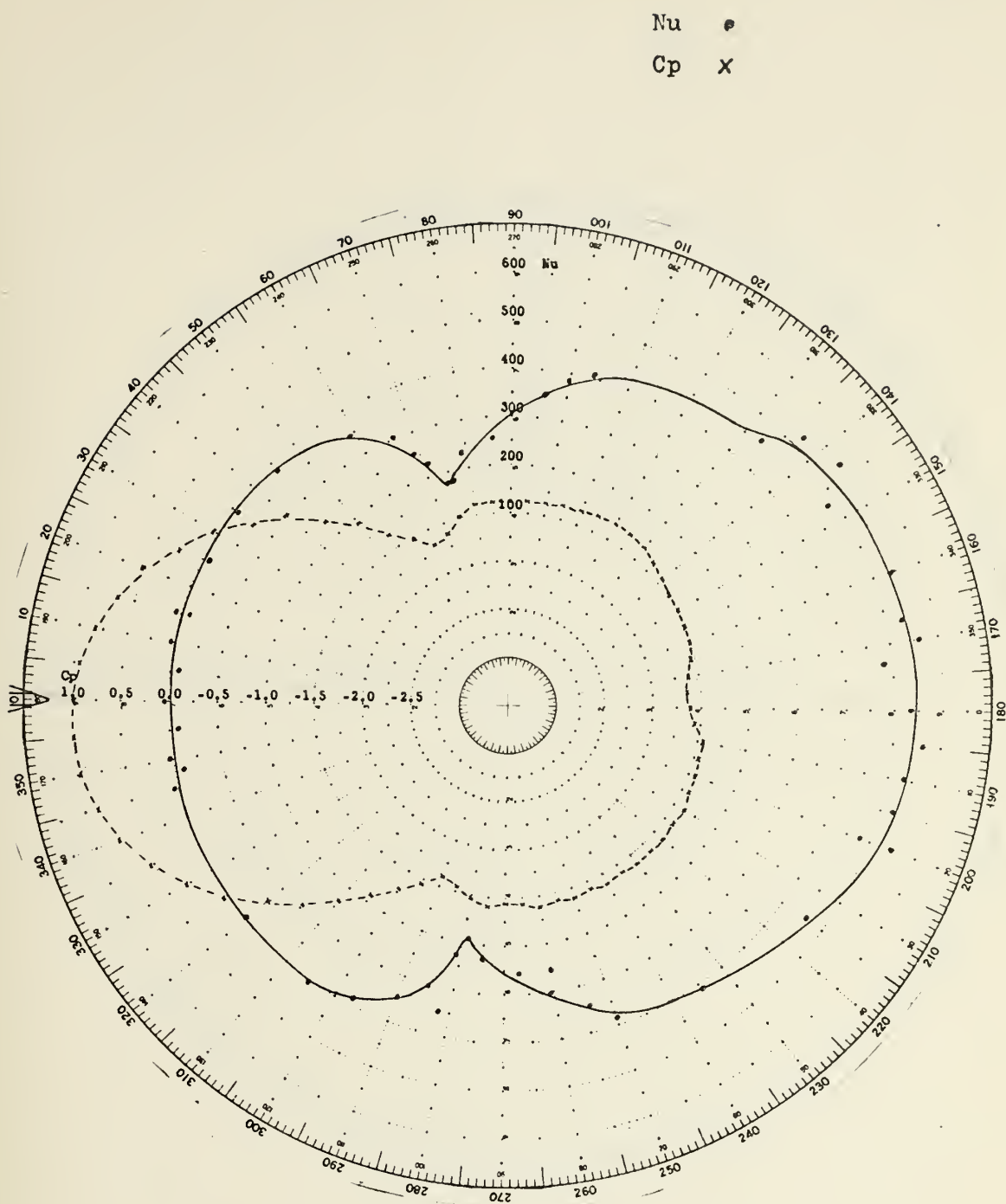


Figure 17. Polar plot of Nusselt number and pressure coefficient versus angle for $d/r = 2.0$.

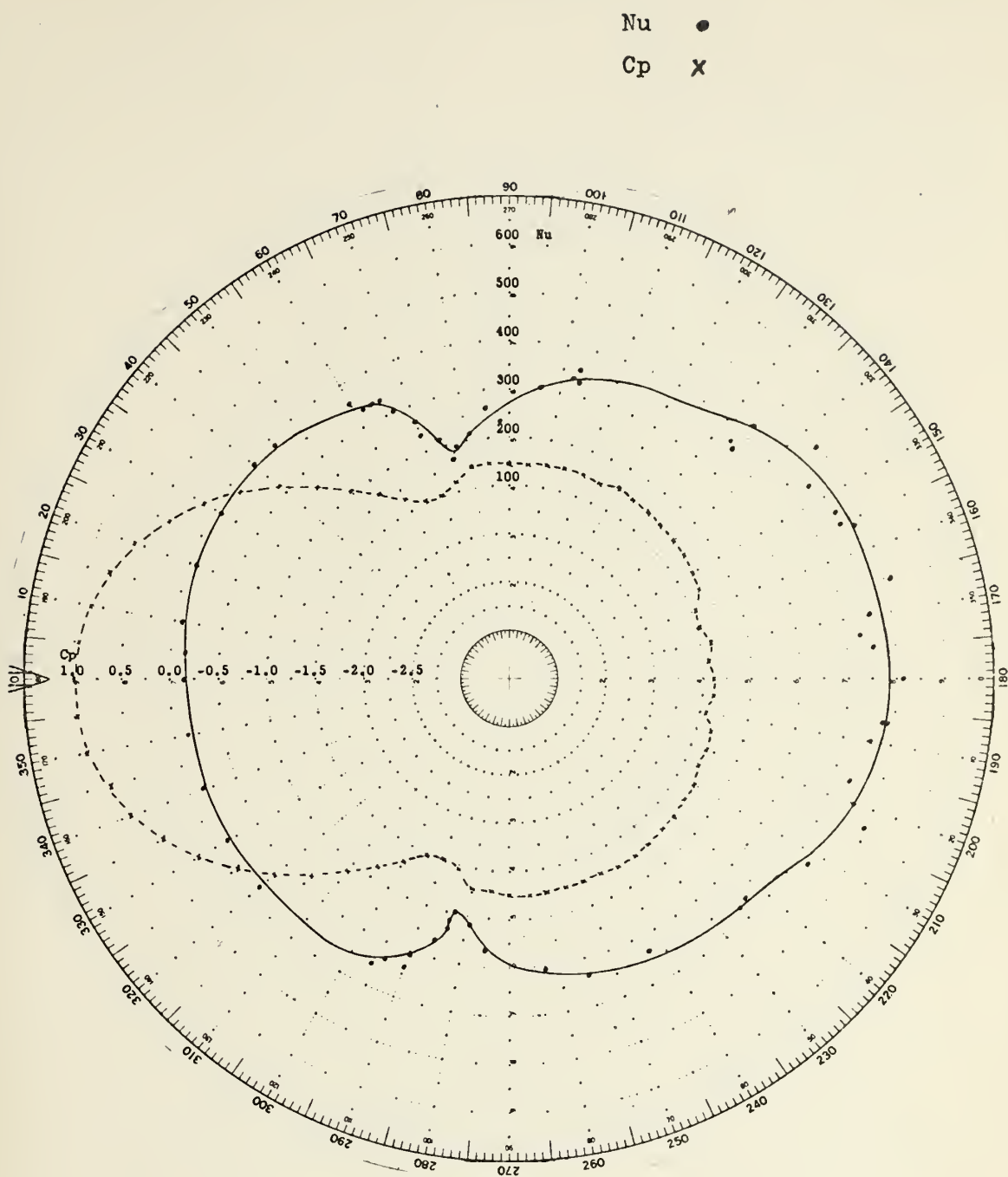


Figure 18. Polar plot of Nusselt number and pressure coefficient versus angle for $d/r = 4.0$.

Nu •
Cp x

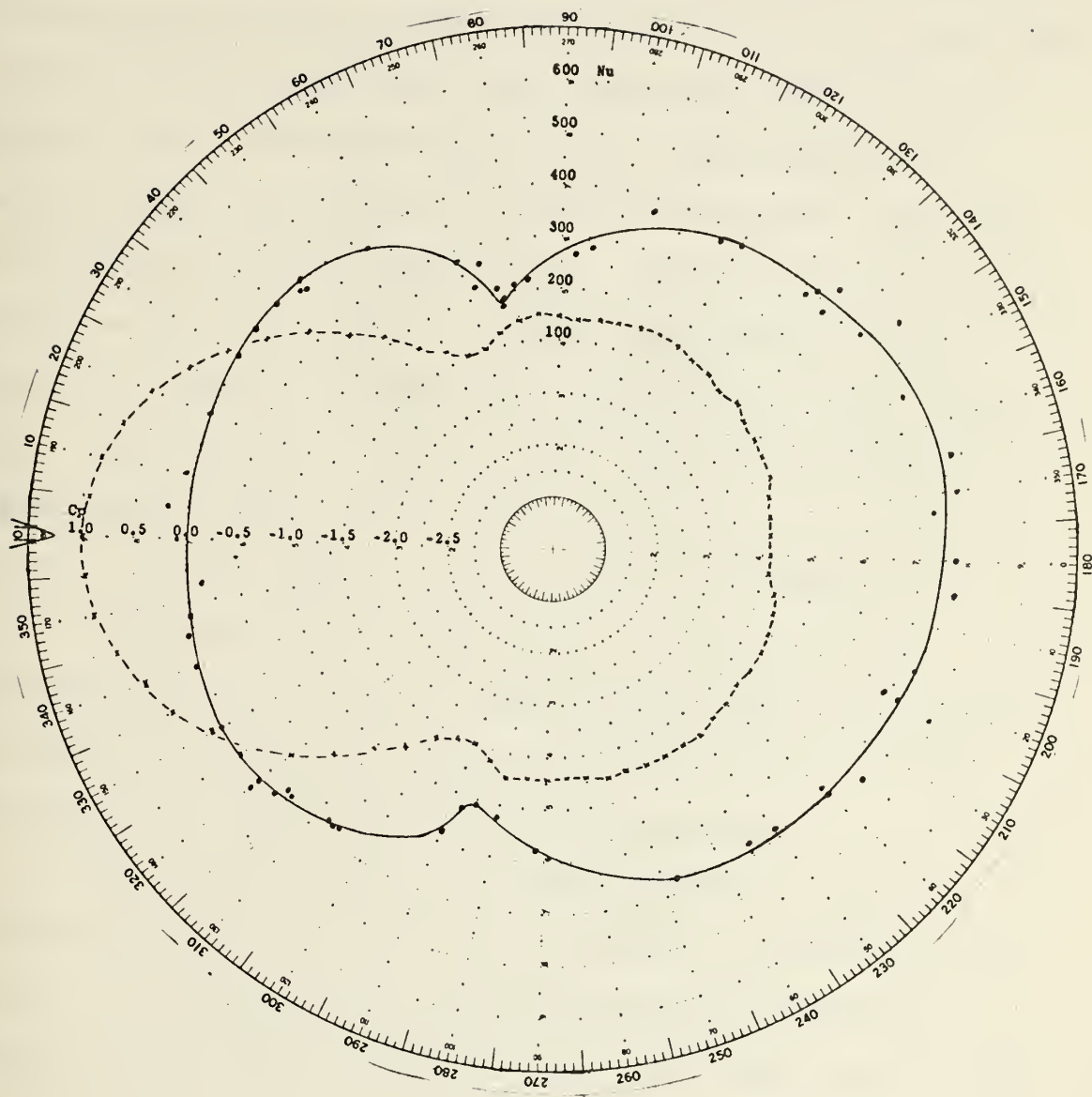


Figure 19. Polar plot of Nusselt number and pressure coefficient versus angle for $d/r = 5.33$.

VI. CONCLUSIONS AND RECOMMENDATIONS

The primary objective of this work, to design, construct and test an experimental apparatus which will allow the study of ground effects on a heated cylinder placed in a cross flow of air, has been achieved. The comparisons made with previous work are within experimental uncertainty, and indicate that the results of further experiments made with this apparatus can be relied upon. The liquid crystal technique for heat transfer analysis has proved to be an excellent method for determining quantitative heat transfer data. The results of the one plate geometry and Reynolds number investigated in this work are shown in the plots of Nu and C_p versus θ . Figure 8 shows the smooth shift in the location of key points which characterize flow phenomena (stagnation point, and laminar separation points) and makes it possible to approximate the value of Nu for configurations other than those investigated.

Future work in this area should include a further investigation of the variation of \overline{Nu} with increasing values of d/r . The first step in this investigation could be further experimentation with the configuration described in this report at various Reynolds numbers. Additional work should also investigate the effect of the plate length on flow patterns. As the wind tunnel used in this work has a capability for flow visualization, a series of experiments to determine flow patterns visually would prove to be valuable.

APPENDIX A

HEAT TRANSFER AND PRESSURE DATA REDUCTION

The equations and procedures used to reduce the heat transfer and pressure data are shown below. The results of each experiment are presented on polar plots of Nu and Cp versus Theta in section V.

A. HEAT TRANSFER EXPERIMENT

The relationship between power dissipated (by convection and radiation heat transfer), and power input by Joulean heating is the same as developed by Field (2) and used by Field and McComas (1).

$$h_t = \frac{V^2}{RA(T-T_\infty)(0.293)}$$

where: h_t = total heat transfer coefficient, $\frac{\text{BTU}}{\text{hr ft}^2 \text{ } ^\circ\text{F}}$

V = voltage applied, volts

R = total resistance of Tensheet, Ohms

A = total heated surface area of Tensheet, Ft^2

T = surface temperature of the cylinder as determined by liquid crystals, $^\circ\text{F}$

T_∞ = air stream temperature, $^\circ\text{F}$

$$0.293 \frac{\text{watt-hr}}{\text{BTU}} = \frac{746 \text{ watts}}{2545 \text{ BTU/hr}}$$

The Nusselt number is defined as:

$$Nu = \frac{h_c d}{K}$$

where:

Nu = Nusselt number

h_c = convection heat transfer coefficient, $\frac{\text{BTU}}{\text{hr ft}^2 \text{ } ^\circ\text{F}}$

d = cylinder diameter, ft

k = $0.015 \frac{\text{BTU}}{\text{hr ft } ^\circ\text{F}}$ (air at 75°)

Since Nu is defined by the convective heat transfer coefficient, it is necessary to subtract the radiation effects from the total heat transfer coefficient

$$h_c = h_t - h_r$$

This correction is made using the equivalent radiation heat transfer coefficient h_r , where h_r is defined as:

$$h_r = \mathcal{F}_{1-2} \sigma (T + T_\infty) (T^2 + T_\infty^2)$$

where:

h_r = equivalent radiation heat transfer coefficient $\frac{\text{BTU}}{\text{hr ft}^2 \text{ } ^\circ\text{F}}$

σ = $0.1714 \times 10^{-8} \frac{\text{BTU}}{\text{hr ft}^2 \text{ } ^\circ\text{R}^4}$ (Stefan-Boltzman Const)

\mathcal{F}_{1-2} = 0.9 radiation exchange factor between the cylinder and the surroundings

T = cylinder surface temperature, °R

T_∞ = air stream temperature, °R

A sample calculation for data obtained at a $Re = 153,000$ and $d/r = 0.50$ is shown below:

$$\theta = 68 \text{ degrees; } V = 24.65 \text{ volts, } T = 111.0^\circ\text{F, } T_\infty = 63.5^\circ\text{F}$$

$$h_t = \frac{24.65^2 \text{ volt}^2}{(13.2n)(0.314 \text{ ft}^2)(111-63.5^\circ\text{F})(.293 \frac{\text{watt hr}}{\text{BTU}})}$$

$$h_t = 10.5 \frac{\text{BTU}}{\text{hr ft}^2^\circ\text{F}}$$

$$h_r = (0.1714 \times 10^{-8} \frac{\text{BTU}}{\text{hr ft}^2^\circ\text{R}^4})(.9)(571 + 523.5^\circ\text{R})$$

$$(571^2 + 523.5^2 \text{R}^2)$$

$$h_r = 1.0 \frac{\text{BTU}}{\text{hr ft}^2^\circ\text{F}}$$

$$h_c = h_t - h_r$$

$$h_c = 9.5 \frac{\text{BTU}}{\text{hr ft}^2^\circ\text{F}}$$

$$Nu = \frac{(9.5 \frac{\text{BTU}}{\text{hr ft}^2^\circ\text{F}})(.25 \text{ ft})}{(.0150 \frac{\text{BTU}}{\text{hr ft}^\circ\text{F}})}$$

$$Nu = 158$$

B. PRESSURE COEFFICIENT EXPERIMENT

As described previously, the pressure coefficient is defined as:

$$C_p = \frac{P - P_\infty}{\frac{1}{2} \rho U_\infty^2} = \frac{P - P_\infty}{P_s - P_\infty}$$

where:

C_p = pressure coefficient

ρ = density of air, lb/ft³

U_∞ = air stream velocity, ft/sec

P = pressure on cylinder surface, in_{H₂O}

P_s = stagnation pressure, in_{H₂O}

P_∞ = air stream pressure, in_{H₂O}

A sample calculation for data obtained at a $Re = 153,000$ and $d/r = 0.50$ is shown below:

$$\theta = 70^\circ \quad P = 10.0 \quad P_\infty = 6.0 \quad P_s = 1.86$$

$$C_p = \frac{10.1 - 6.0}{1.86 - 6.0}$$

$$C_p = - 0.99$$

APPENDIX B
UNCERTAINTY ANALYSIS

Because of the uncertainties in the measured variables, it was necessary to perform an uncertainty analysis in order to ascertain the degree of uncertainty in the experimental results. The method of Kline and McClintock (7) was used.

The following estimated uncertainties existed:

voltage, V	± 0.1 volts	(20:1)
resistance, R	± 0.2 ohms	(20:1)
temperature ΔT	$\pm 1.0^\circ\text{F}$	(20:1)
area A	± 0.01 ft ²	(20:1)
diameter d	± 0.001 ft	(20:1)
radiation exchange factor \mathcal{F}	± 0.05	(20:1)
wall manometer H	± 0.05 in	(20:1)
manometer bank S	± 0.05 in	(20:1)

Total Heat Transfer Coefficient, h_t :

As shown in Appendix A, the equation used to calculate the total heat transfer coefficient was:

$$h_t = \frac{V^2}{RA(T - T_\infty)}$$

(since the conversion from watts to BTUs is a constant, it does not enter into the uncertainty analysis).

For data obtained at a Reynolds number of 153,000
and $d/r = 0.50$:

$$V = 24.65 \pm 0.1 \text{ volts}$$

$$R = 13.2 \pm 0.3 \text{ ohms}$$

$$\Delta T = 47.5 \pm 1.0 \text{ } ^\circ\text{F}$$

$$A = 0.315 \pm 0.001 \text{ ft}^2$$

$$\frac{\omega_{h_t}}{h_t} = \sqrt{\left(\frac{2\omega_v}{V}\right)^2 + \left(\frac{\omega_R}{R}\right)^2 + \left(\frac{\omega_A}{A}\right)^2 + \left(\frac{\omega_{\Delta T}}{\Delta T}\right)^2}$$

$$\frac{\omega_{h_t}}{h_t} = 0.03 \text{ or } \omega_{h_t} = \pm 0.3$$

$$h_t = 10.5 \pm 0.3$$

In some regions where $T = \pm 2.0 \text{ } ^\circ\text{F}$, then:

$$\frac{\omega_{h_t}}{h_t} = 0.05 \text{ or } \omega_h = 0.5$$

$$h = 10.5 \pm 0.5$$

All measured quantities were read with the uncertainties shown above, with the result that the calculated value of total heat transfer coefficient had a relatively constant value around the circumference of the cylinder.

Since the angular location of the color bands does not enter into the calculation of H_t , the angular uncertainty has not been included here. This uncertainty is estimated to be ± 3 degrees.

Equivalent Radiation Heat Transfer Coefficient, h_r :

The equation used to calculate H_r was:

$$h_r = \sigma \mathcal{F}(T + T_\infty)(T^2 + T_\infty^2)$$

defining $T_m = 1/2 (T + T_\infty)$

$$h_r = 4\sigma \mathcal{F} T_m^3$$

since σ is a constant, it does not enter into the uncertainty analysis.

For the same data used to perform the uncertainty analysis for h_t , the uncertainty in h_r was found to be:

$$\frac{\omega_{h_r}}{h_r} = \sqrt{\left(\frac{\omega_{\mathcal{F}}}{\mathcal{F}}\right)^2 + \left(\frac{3 \omega_{T_m}}{T_m}\right)^2}$$

$$\frac{\omega_{h_r}}{h_r} = 0.06 \text{ or } \omega_{h_r} = 0.06$$

$$h_r = 1.00 \pm 0.06$$

Nusselt Number, Nu:

The equation used to calculate Nu was:

$$Nu = \frac{h_c d}{k}$$

$$\text{where } h_c = h_t - h_r$$

since k is a property of air, and its uncertainty is negligible:

$$\frac{\omega_{Nu}}{Nu} = \sqrt{\left(\frac{\omega_{h_c}}{h_c}\right)^2 + \left(\frac{\omega_d}{d}\right)^2}$$

$$\omega_{h_c} = \sqrt{\omega_{h_t}^2 + \omega_{h_r}^2} \approx \omega_{h_t}$$

$$\frac{\omega_{Nu}}{Nu} = 0.03 \quad \text{or} \quad \omega_{Nu} = \pm 5$$

$$Nu = 158 \pm 5$$

While this analysis has shown that $\frac{\omega_{Nu}}{Nu} = 0.03$, and $\theta = \pm 3$ degrees, it should be noted that this may be misleading. Because there are portions of the cylinder which exhibit different flow phenomena, there are different types of color bands exhibited. The isothermal region has no distinct bands, and the mottled colors which appear cover a wide area. The liquid crystals were calibrated with

respect to the onset of each color. The result is that for areas of pulsating or mottled colors, the uncertainty of surface temperature and location are much higher than for regions in which a distinct color gradient exists.

Reynolds Number, Re:

The equation used to calculate Re was:

$$Re = \frac{U_{\infty} d}{\nu}$$

The value of U_{∞} is directly proportional to the square root of the wall manometer reading, therefore:

$$\frac{\omega U_{\infty}}{U_{\infty}} = 0.5 \frac{\omega_H}{H}$$

since ν is a property of air, and its uncertainty is negligible:

$$\frac{\omega_{Re}}{Re} = \sqrt{\left(\frac{0.5 \omega_H}{H}\right)^2 + \left(\frac{\omega_d}{d}\right)^2}$$

$$\frac{\omega_{Re}}{Re} = 0.011 \quad \text{or} \quad \omega_{Re} = 1700 \approx 2000$$

$$Re = 153,000 \pm 2000$$

Pressure Coefficient, C_p :

The equation used to calculate C_p was:

$$C_p = \frac{P - P_s}{P_\infty - P_s} = \frac{\Delta P_1}{\Delta P_2}$$

both pressure differences were measured on the same manometer bank. For $Re = 153,000$ and $d/r = 0.50$:

$$P = 10.1 \quad P_\infty = 6.0 \quad P_s = 1.86$$

$$\frac{\omega C_p}{C_p} = \sqrt{\left(\frac{\omega \Delta P_1}{\Delta P_i}\right)^2 + \left(\frac{\omega \Delta P_2}{\Delta P_2}\right)^2}$$

$$\frac{\omega C_p}{C_p} = 0.017 \quad \text{or} \quad \omega C_p = 0.017 \approx 0.02$$

$$C_p = -0.99 \pm 0.02$$

APPENDIX C

HOT WIRE ANEMOMETER CALIBRATION

Prior to any experimental runs, the TSI hot wire anemometer was calibrated using a controlled air stream and a precision manometer. In order to assure accurate calibration, the probe was mounted in the wind tunnel traversing mechanism and the calibration was done in the wind tunnel test section. In this way all leads and connections used for experimental runs would be in the circuit for calibration.

The calibration apparatus provided a controlled air flow whose velocity was calculated from the pressure differential provided by an alcohol-filled manometer. The velocity calculated was plotted against the voltage indicated by the hot wire anemometer unit (Figure 20). Calibration was done by increasing the calibration apparatus air stream velocity so that the alcohol in the manometer would indicate even values (in mm). The manometer inclination and readings were recorded, along with the voltage indicated by the hot wire anemometer.

The equations used, data taken and calibration curves are shown below. Calibration checks were made periodically throughout the course of this work, and corrections made to account for the aging of the probe.

From Bernoulli's Equation:

$$U_{\infty} = \sqrt{\frac{2 g_c \Delta P}{\rho}}$$

where:

U_{∞} = air stream velocity ft/sec

g_c = 32.17 ft/sec²

ρ = air density lb/ft³

ΔP = pressure differential lb/ft²

The pressure differential from the manometer was calculated from the following relations:

$$P = \frac{\rho_{H_2O} g}{g_c} h$$

and $h = \frac{0.789}{0.80} c h'$

where:

$\frac{0.789}{0.80}$ = ratio of specific gravity of manometer fluid used, to specific gravity of fluid intended for manometer

c = manometer inclination factor

h' = height of meniscus in inclined manometer mm

hence:

$$U_{\infty} = 13.24 \sqrt{h} \text{ ft/sec}$$

where:

h = mm of alcohol

Turbulence intensity was determined by:

$$T_u = \frac{4 V e}{V^2 - V_0^2}$$

where:

T_u = turbulence intensity

V = voltage indicated by hot wire anemometer

e = rms voltage variation

V_0 = extrapolated value of voltage corresponding to zero velocity

Hot Wire Anemometer Calibration

c inclination	h mm	h mm H ₂ O	v v _{ell}	e v _{ell}	u mm/sec	\sqrt{u}	$\sqrt{v^2}$
0.05	20.0	0.986	2.446	0.0015	13.147	3.626	7.001
	40.0	1.972	2.762	0.0013	15.583	4.312	7.629
	60.0	2.958	2.830	0.0012	22.771	4.772	8.009
	80.0	3.944	2.884	0.0011	26.294	5.128	8.317
	100.0	4.93	2.930	0.0011	29.378	5.422	8.585
	150.0	7.375	3.010	0.0011	36.005	6.000	9.000
	200.0	9.86	3.074	0.0011	41.574	6.448	9.449
0.1	100.0	9.86	3.072	0.0011	41.574	6.448	9.437
	150.0	14.79	3.164	0.0011	50.918	7.136	10.011
	200.0	19.72	3.231	0.0011	58.795	7.668	10.439
0.2	100.0	19.72	3.229	0.0010	58.795	7.668	10.426
	150.0	29.58	3.325	0.0012	72.009	8.486	11.056
	200.0	39.44	3.391	0.0025	83.149	9.119	11.479
0.4	100.0	39.44	3.391	0.0025	83.149	9.119	11.479
	150.0	59.16	3.497	0.0019	101.836	10.091	12.229
	200.0	78.88	3.570	0.0019	117.570	10.844	12.745
0.8	100.0	78.88	3.575	0.0016	117.590	10.844	12.781
	200.0	157.76	3.762	0.0022	166.298	12.896	14.153

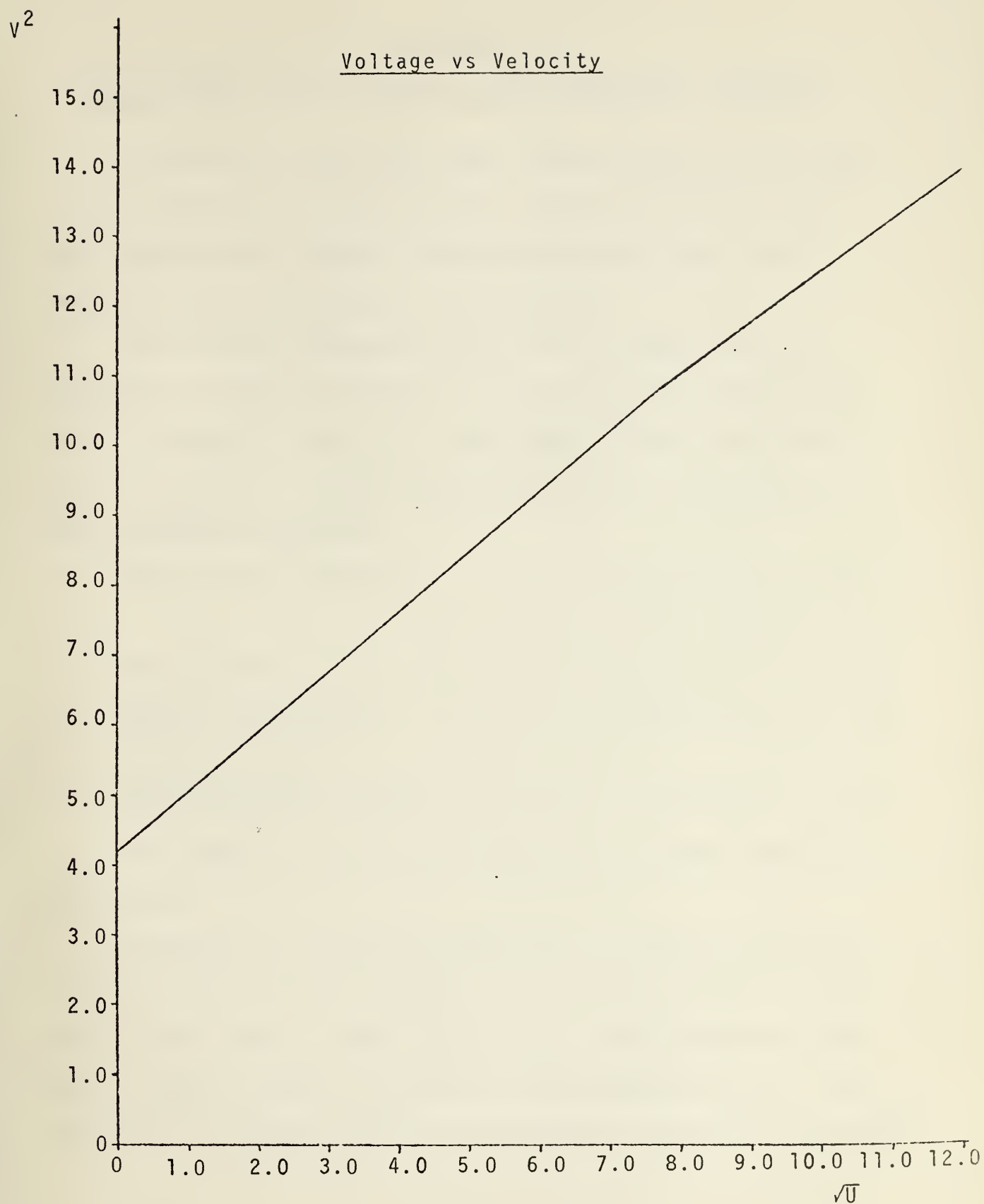


Figure 20. Voltage squared versus the square root of velocity for hot wire anemometer calibration.

APPENDIX D

WIND TUNNEL VELOCITY PROFILE AND TURBULENCE INTENSITY

In order to assure that test results would be accurate, it was necessary to show that the velocity profile in the test section was constant and that turbulence was small enough to have no effect on test results.

The hot wire anemometer was used to probe the test section at various locations. The test section coordinate axis is shown in Figure 21. The test cylinder was located at $X = 13.71$, $Y = -2.33$. Velocity profiles were taken at the following locations:

Test section entrance: $X = 17.75$ $-9.0 \leq Y \leq +9.0$ $Z = 0.0$

$X = 17.75$ $Y = -2.2 \leq +4.0 \leq Z = 4.0$

Plate leading edge: $X = -1.71$ $-3.023 \leq Y \leq +9.0$ $Z = 0.0$

Top of the cylinder:
(plate attached) $X = -13.71$ $-0.825 \leq Y \leq +9.0$ $Z = 0.0$

Top and bottom of cyl.: $X = -13.71$ $-10.0 \leq Y \leq +9.0$ $Z = 0.0$
(plate at $d/r = 5.33$)

All velocity profiles were taken at a tunnel speed of 98 ft/sec.

As shown in Figures 22 and 23 the air speed increased from 10 to 30 percent on either side of the cylinder in the case of the plate at $d/r = 5.33$, and a like amount over the top of the cylinder in the case of the attached plate. The velocity at the test section entrance was essentially constant.

Turbulence intensity was determined at the test section entrance:

$$X = 17.7 \quad -5.0 \leq Y \leq +5.0 \quad Z = 0.0$$

for three Reynolds numbers; 75,000, 100,000, and 153,000. The average value of turbulence intensity for $Re = 153,000$ was 0.00239, or about 0.2%. The turbulence for the other Reynolds numbers was slightly higher, but of the same order of magnitude (see data). The value of turbulence intensity was calculated in the same manner as for the hot wire anemometer probe calibration described in Appendix C.

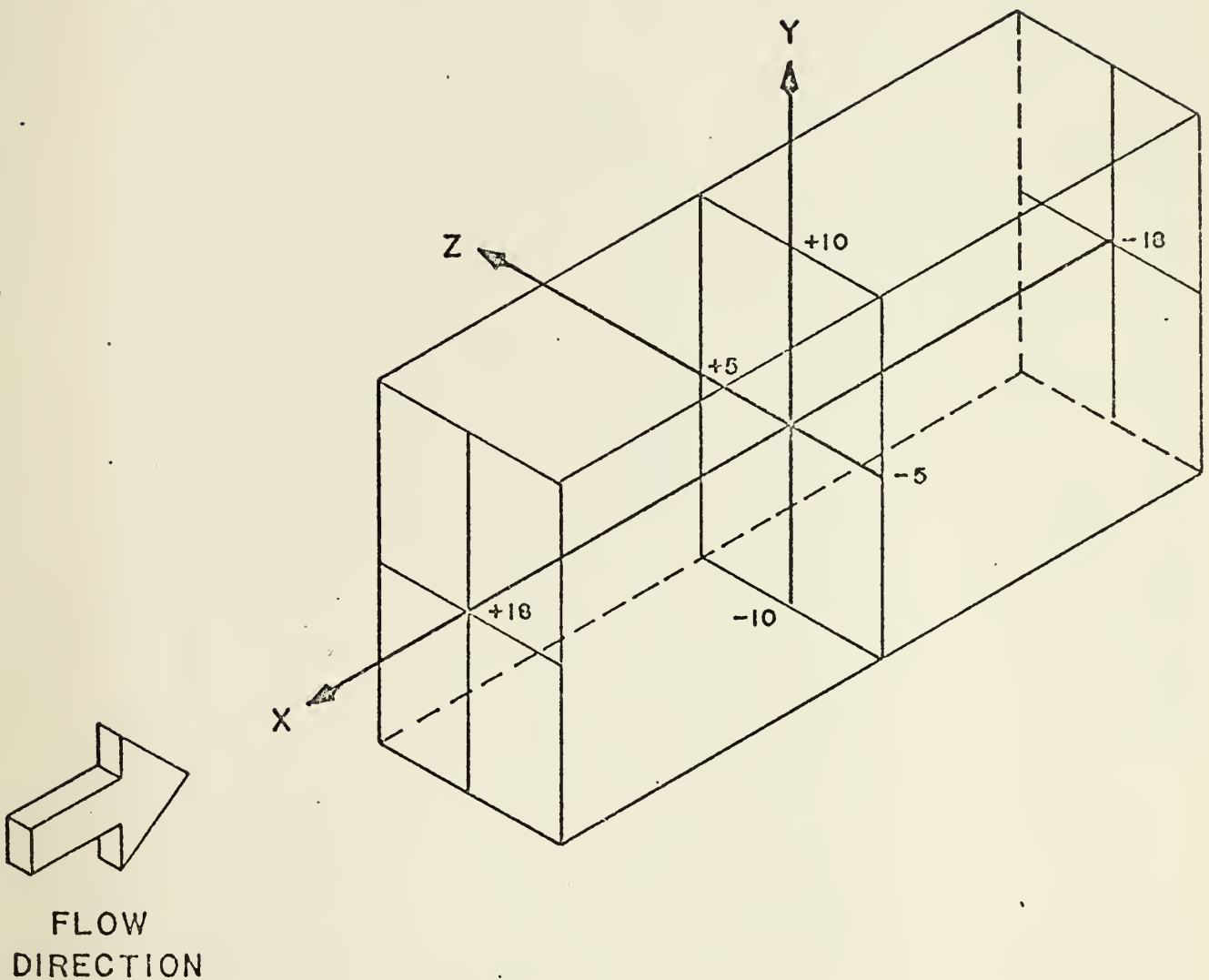
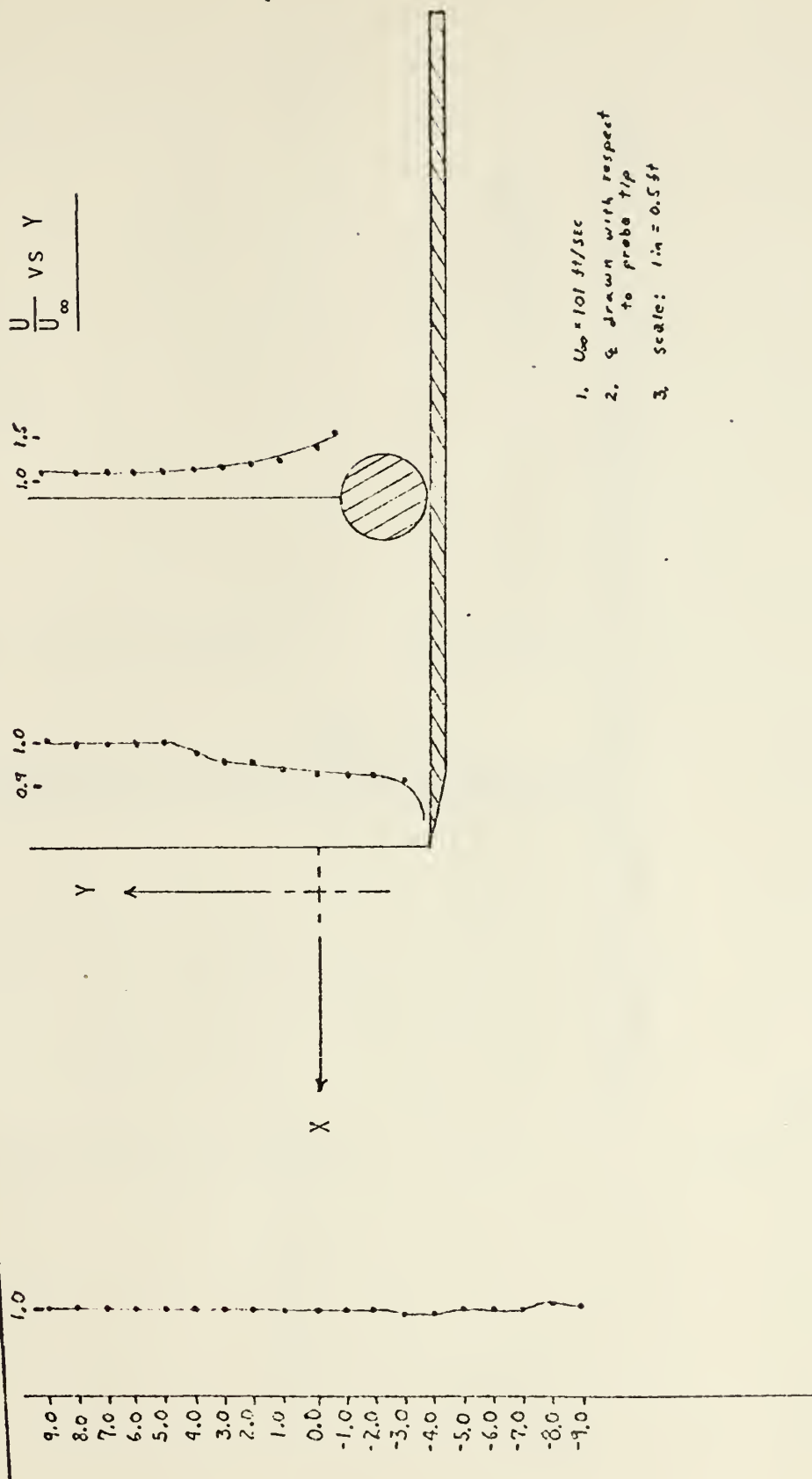


Figure 21. Isometric of the test section coordinate axis.

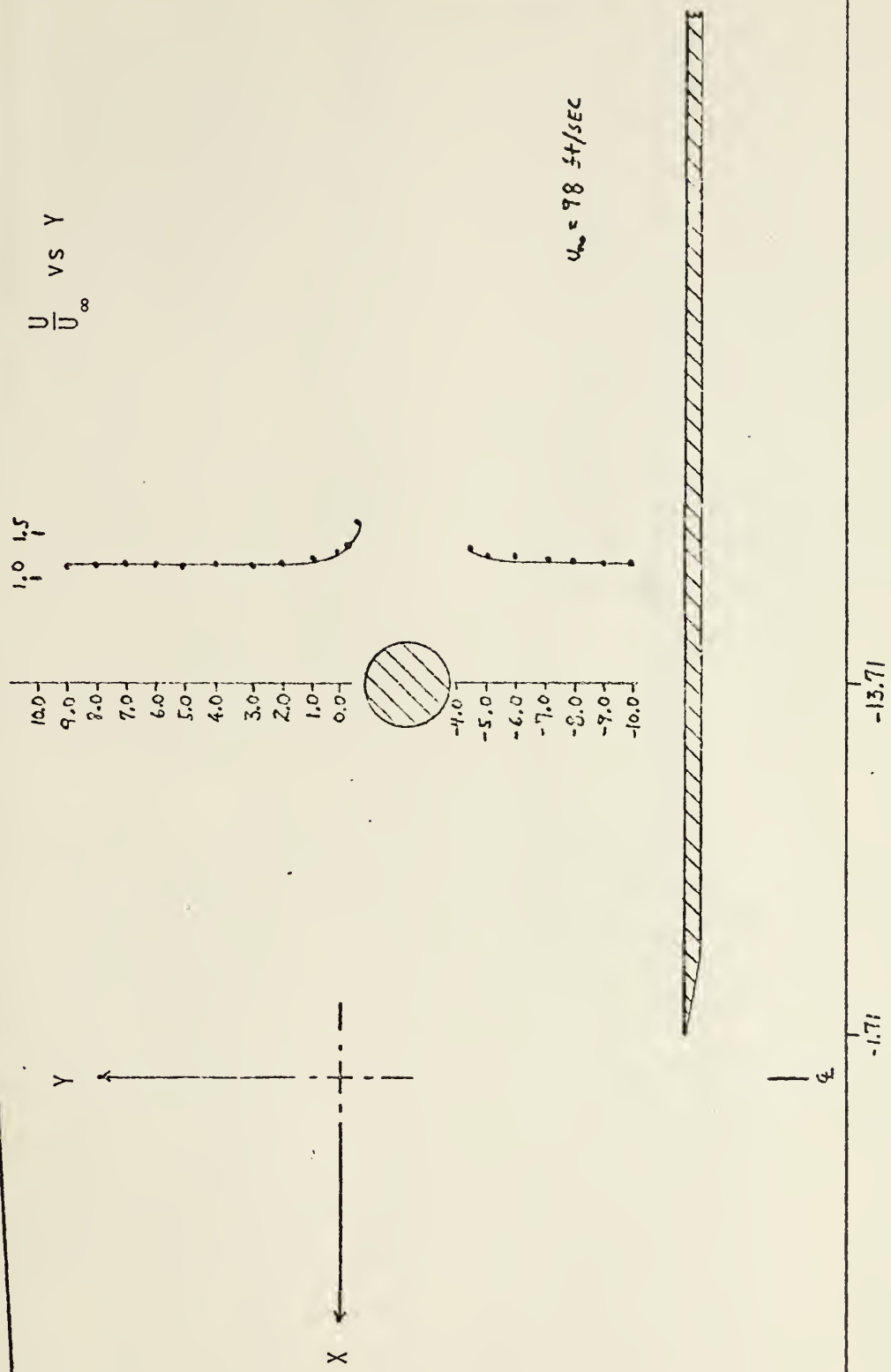


17.7

0.0-1.71

-13.71

Figure 22. Velocity profiles at the test section entrance, Plate leading edge, and the top of the cylinder for $d/r = 0.0$.



VELOCITY PROFILES

69

22 11 1891

70

Turbulence Intensity

Re	Y	V_{rms}	e_v	V_0	T_u	$Av T_u$		
15,000	-5.0	3.532	0.0035	2.05	0.00256			
	0.0	3.536	0.0033	2.05	0.00222			
	5.0	3.540	0.0034	2.05	0.00238	0.00239		
100,000	5.0	3.330	0.0031	2.05	0.00213			
	0.0	3.236	0.0031	↓	0.00212			
	-5.0	3.341	0.0031	↓	0.00211	0.00212		
75,000	-5.0	3.231	0.00395	2.05	0.00404			
	0.0	3.220	0.0040	↓	0.00418			
	5.0	3.213	0.0031		0.00231	0.00351		
NOTE:								
① Electronics Noise = .002								
<u>Subt off all above values of e_v</u>								
② Readings taken at:								
$X = 17.7$								
$Y = \text{various}$								
$Z = 0.0$								

LIST OF REFERENCES

1. McComas, J.P., Experimental Investigation of Ground Effects on a Heated Cylinder in Crossflow, MSME Thesis, Naval Postgraduate School, 1974.
2. Field, R.J., Liquid Crystal Mapping of the Surface Temperature on a Heated Cylinder Placed in a Crossflow of Air, MSME Thesis, Naval Postgraduate School, 1974.
3. Naval Postgraduate School Report NPS-59Cg 74111, A Liquid Crystal Thermographic Study of a Heated Cylinder in Cross Flow, by T.E. Cooper, R.J. Field, and J.F. Meyer, November, 1974.
4. Pope, A., Wind-Tunnel Testing, 2d. ed., p. 268-286, Wiley and Sons, 1954.
5. Meyer, J.F., An Experimental Investigation of the Heat Transfer Characteristics of a Heated Cylinder Placed in a Crossflow of Air, ENGR Thesis, Naval Postgraduate School, 1973.
6. Armed Services Technical Information Agency, AD 66184, "A New Method for Calculating Laminar Heat Transfer on Cylinders of Arbitrary Cross-Section and on Bodies of Revolution at Constant and Variable Wall Temperatures," Schuh, 1953.
7. Kline, S.J. and McClintock, F.A., "Describing Uncertainties in Single-Sample Experiments," Mechanical Engineering, v. 75, p. 3-8, January 1953.

INITIAL DISTRIBUTION LIST

	No. Copies
1. Defense Documentation Center Cameron Station Alexandria, VA 22314	2
2. Library, Code 0212 Naval Postgraduate School Monterey, CA 93940	2
3. Department Chairman, Code 59 Department of Mechanical Engineering Naval Postgraduate School Monterey, CA 93940	1
4. T.E. Cooper, Code 59Cg Department of Mechanical Engineering Naval Postgraduate School Monterey, CA 93940	3
5. LT Charles H. Gnerlich, USN c/o Commanding Officer Surface Warfare Schools Command Newport, Rhode Island 30465	1
6. C.F. Markarian Code 4061 Naval Weapons Center China Lake, CA 93555	1

15 AUG 75

22803

160774

Thesis
G521
c.1

Gnerlich
The convective heat
transfer behavior of a
heated cylinder loca-
ted near a plane sur-
face.

15 AUG 75

160774

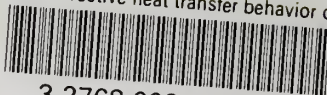
Thesis
G521
c.1

Gnerlich

The convective heat
transfer behavior of a
heated cylinder loca-
ted near a plane sur-
face.

thesG521

The convective heat transfer behavior of



3 2768 002 02958 9

DUDLEY KNOX LIBRARY